Article type: **Research Advances**

TEAD1 is crucial for developmental myelination, Remak bundles, and functional regeneration of peripheral nerves

Matthew Grove[1], Hyukmin Kim[1], Shuhuan Pang[1], José Paz Amaya[2], Guoqing Hu[3], Jiliang Zhou[3], Michel Lemay[2], and Young-Jin Son[1]*

[1]Department of Neural Sciences, Shriners Hospitals Pediatric Research Center, Lewis Katz School of Medicine, Temple University, Philadelphia, PA 19140

[2]Department of Bioengineering, Temple University, Philadelphia, PA 19122, USA

[3]Department of Pharmacology & Toxicology, Medical College of Georgia, Augusta University, Augusta, GA

* Corresponding author: yson@temple.edu

ABSTRACT

Previously we showed that the hippo pathway transcriptional effectors, YAP and TAZ, are essential for Schwann cells (SCs) to develop, maintain and regenerate myelin (Grove et al., 2017; Grove, Lee, Zhao, & Son, 2020). Although TEAD1 has been implicated as a partner transcription factor, the mechanisms by which it mediates YAP/TAZ regulation of SC myelination are unclear. Here, using conditional and inducible knockout mice, we show that TEAD1 is crucial for SCs to develop and regenerate myelin. It promotes myelination by both positively and negatively regulating SC proliferation, enabling Krox20/Egr2 to upregulate myelin proteins, and upregulating the cholesterol biosynthetic enzymes FDPS and IDI1. We also show stage-dependent redundancy of TEAD1 and that non-myelinating SCs have a unique requirement for TEAD1 to enwrap nociceptive axons in Remak bundles. Our findings establish TEAD1 as a major partner of YAP/TAZ in developmental myelination and functional nerve regeneration and as a novel transcription factor regulating Remak bundle integrity.

INTRODUCTION

In the mammalian peripheral nervous system, all motor and sensory axons are associated with Schwann cells (SCs). Axons larger than 1μm diameter are enveloped by myelinating SCs that form multilamellar myelin sheaths with a thickness proportional to axon caliber (Jessen & Mirsky, 2005; Salzer, 2015). Axons smaller than 1μm diameter, the unmyelinated nociceptors (i.e., C-fibers), are organized in clusters called Remak bundles, in which each C-fiber is ensheathed by a cytoplasmic pocket formed by non-myelinating SCs, also known as Remak SCs (Beirowski et al., 2014; Harty & Monk, 2017). Both myelinating and non-myelinating SCs provide metabolic and functional support essential for structural and functional integrity of peripheral nerves. Failure to initiate or maintain proper axon-SC association may lead to life-threatening paralysis and peripheral neuropathy (Scherer & Wrabetz, 2008). Myelinating SCs form and maintain myelin via a set of key transcription factors (TFs) and regulators (Bremer et al., 2011; Decker et al., 2006; Finzsch et al., 2010; Y. He et al., 2010; Jaegle et al., 2003; Kao et al., 2009; Le, Nagarajan, Wang, Svaren, et al., 2005). However, the transcriptional regulation of myelinating SCs remains incompletely understood, and that of non-myelinating SCs is largely unknown (Harty & Monk, 2017).

Recent mouse genetic studies surprisingly revealed that YAP (Yes-associated protein, also known as YAP1) and its paralogue, TAZ (Transcriptional coactivator with PDZ-binding motif, also known as WWTR1), which are potent oncoproteins and transcriptional regulators in the Hippo signaling pathway, play crucial roles in developing, maintaining, and regenerating myelination of peripheral nerves. Both YAP and TAZ (YAP/TAZ) are expressed initially in all immature SCs and then selectively in myelinating SCs (Grove et al., 2017). The processes for which they are required include: timely sorting of large axons and associated SC proliferation (Grove et al., 2017; Poitelon et al., 2016); initiation of SC differentiation or myelination (Deng et al., 2017; Grove et al., 2017); myelin maintenance in adults (Grove et al., 2017); and remyelination following nerve injury (Grove et al., 2020; Jeanette et al., 2021). YAP/TAZ initiate and maintain myelination in part by upregulating Krox20 (Egr2) (Grove et al., 2017; Lopez-Anido et al., 2016), which is widely recognized as the master TF promoting peripheral myelination by SCs. Krox20 is required to develop and maintain myelin (Decker et al., 2006; Topilko et al., 1994), and likely to promote myelin sheath growth (Le, Nagarajan, Wang, Araki,

69 et al., 2005). It acts through direct transcriptional upregulation of myelin proteins and membrane
70 lipids (Jang et al., 2010; Jang & Svaren, 2009; LeBlanc, Jang, Ward, Wrabetz, & Svaren, 2006).
71 YAP/TAZ are transcriptional co-activators that contain a transcriptional activation
72 domain, but no DNA binding domain. They regulate gene expression by binding to partner TFs,
73 typically members of the TEA domain family (TEAD1-4) (Wu, Liu, Zheng, Dong, & Pan, 2008;
74 Zhao et al., 2008). Conversely, TEADs on their own are unable to activate or repress
75 transcription and require the help of co-factors such as YAP/TAZ to act (Li et al., 2010; Tian,
76 Yu, Tomchick, Pan, & Luo, 2010). Partner TFs such as TEADs are required to maintain
77 YAP/TAZ in the nucleus, which keeps them transcriptionally active (Diepenbruck et al., 2014; J.
78 Kim et al., 2020; Kofler et al., 2018; Yao et al., 2018). Recent single cell transcriptional analysis
79 indicates that SCs express all four TEADs (TEAD1/2/3/4) and that their expression peaks at
80 different times during development (Gerber et al., 2021). Moreover, TEAD1-4 show unique,
81 redundant, and/or opposing roles in regulating proliferation and differentiation of various cell
82 types; these roles can also change as a function of developmental stage (X. He et al., 2018;
83 Mukhtar et al., 2020). It remains to be elucidated how and which TEAD(s) in SCs mediate
84 transcriptional regulation of YAP/TAZ for the development, maintenance, and/or regeneration of
85 myelination after nerve injury.
86 In some cell types, TEAD1 serves as the main partner TEAD and plays non-redundant
87 roles (Liu et al., 2019; Wen et al., 2019). In accordance, in SCs, TEAD1 associates with
88 YAP/TAZ for upregulating myelin proteins as indicated by ChiP, co-IP, and transcription assays
89 (Fernando et al., 2016; Grove et al., 2017; Lopez-Anido et al., 2016; Lopez-Anido et al., 2015).
90 Notably, however, unlike YAP/TAZ, which are barely detectable in non-myelinating SCs,
91 TEAD1 is clearly expressed in all SC nuclei (Grove et al., 2017), suggesting that, independently
92 of YAP/TAZ, TEAD1 plays an unknown role in non-myelinating SCs. In this study, we
93 generated conditional and inducible knockout mice lacking TEAD1 in SCs to investigate the
94 roles of TEAD1 in myelinating and non-myelinating SCs. We found that TEAD1 is required for
95 myelinating SCs to form, grow, and regenerate myelin, and for non-myelinating SCs to enwrap
96 C-fibers in Remak bundles during development and homeostasis. We also found that YAP/TAZ-
97 TEAD1 promotes myelination by dually regulating SC proliferation, by enabling induced
98 Krox20 to upregulate myelin proteins, and by upregulating cholesterol biosynthetic enzymes.
99

100 **RESULTS**

101

102 **Multiple TEADs are expressed in Schwann cells of WT and *Tead1* cKO mice**

103 To investigate the roles of SC TEAD1 in developing nerves, we conditionally ablated
104 *Tead1* by crossing *Tead1*$^{fl/fl}$ mice (Wen et al., 2017) with mice carrying *Mpz*-Cre, which is active
105 from E13.5 in SCs (Feltri et al., 1999). Immunostaining of P22 WT and *Mpz-Cre;Tead1*$^{fl/fl}$
106 (hereafter *Tead1* cKO) sciatic nerves (SNs) showed that TEAD1 was expressed in the nuclei of
107 100% of WT SCs and was undetectable in >97% *Tead1* cKO SCs (Figure 1A). The specificity of
108 the TEAD1 immunostaining and highly efficient deletion were further confirmed by Western
109 blotting (Figure 1B).

110 To investigate the protein expression of other TEADs, we used antibodies to TEAD2, 3,
111 and 4, and a pan-TEAD antibody marketed as recognizing all four TEADs (TEAD1/2/3/4).
112 Western blot analysis of SN lysates showed that anti-TEAD3 and anti-pan TEAD both contained
113 a main ~ 50kD band that was decreased in *Tead1* cKO (Figure 1B). The pan-TEAD antibody
114 may therefore bind preferentially to TEAD3. Anti-TEAD4 recognized three bands in WT and
115 showed that the two faster-migrating bands were decreased in *Tead1* cKO. Anti-TEAD2
116 recognized a band of ~65 kD in *Tead1* cKO that was barely detectable in WT lysates. This band
117 corresponded to the size of TEAD2 reported in other cell types (Beverdam et al., 2013). We also
118 found that the ~65 kD band was present early postnatally, but rapidly diminished with age
119 (Figure 1-figure supplement 1), in accordance with the transcript data from mouse SCs (Gerber
120 et al., 2021). Thus, the expression of TEADs 2-4 was altered in *Tead1* cKO, likely reflecting
121 their expression in SCs, consistent with the single cell transcriptomic analysis of SCs (Gerber et
122 al., 2021). Of these anti-TEAD antibodies, only anti-pan TEAD functioned for
123 immunofluorescence staining, verifying the presence of other TEADs in SC nuclei lacking
124 TEAD1 (Figure 6-figure supplement 1C, 1E).

125 In the absence of a partner TF, nuclear YAP/TAZ are decreased and phosphorylation of
126 YAP/TAZ increased, due to targeting by Large tumor suppressor kinase 1/2 (LATS1/2), negative
127 regulators of YAP/TAZ (Hao, Chun, Cheung, Rashidi, & Yang, 2008; Zhao et al., 2007). To
128 investigate if YAP/TAZ are in the nuclei of SCs and therefore remain transcriptionally functional
129 in the absence of TEAD1, we compared Western blotting of P50 WT vs *Tead1* cKO SN lysates
130 and observed an overall decrease in YAP levels in *Tead1* cKO but a > 2-fold increase in TAZ

131 levels compared to WT (Figure 1C). This ratio of TAZ to YAP in *Tead1* cKO resembled that
132 observed during developmental myelination in WT SNs (Deng et al., 2017; Grove et al., 2017).
133 Furthermore, phosphorylation of YAP decreased in *Tead1* cKO, which would typically indicate
134 increased YAP activity. Thus, YAP/TAZ are not targeted for destruction in the absence of
135 TEAD1 in SCs. Indeed, YAP/TAZ were retained in the SC nucleus of *Tead1* cKO (Figure 1D),
136 presumably due to other TEADs in the absence of TEAD1.
137
138 **TEAD1 is required for myelin formation and growth**
139 *Tead1* cKO mice were smaller than WT mice at all ages, with labored breathing and
140 widely splayed fore- and hindlimbs, indicative of severe peripheral neuropathy (Figure 2A,
141 Video 1). Because of the neuropathy, *Tead1* cKO mice were humanely euthanized before P60.
142 *Tead1* cKO SNs were noticeably translucent, indicative of reduced myelin content (Figure 2B).
143 Electrical stimulation of cKO SNs elicited low and dispersed compound muscle action potentials
144 (CMAPs) (Figure 2C). Nerve conduction velocity (NCV) in cKO was ~8 m/s, which was
145 markedly reduced from ~40 m/s in WT mice (Figure 2D).
146 Next, we used semi-thin and transmission electron microscopy (TEM) to examine the
147 processes of developmental myelination and Remak bundle formation. We first examined SNs at
148 P3, when, in WT, many large axons had already been radially sorted, establishing 1:1
149 relationship with promyelinating SCs, and myelination had begun. Compared to WT, *Tead1* cKO
150 SNs were thinner, unsorted bundles of axons were larger and more numerous, and myelination
151 was minimal (Figure 2E). Nevertheless, we frequently observed large axons that had been sorted
152 and established a 1:1 relationship with promyelinating SCs, as in WT. Therefore, radial sorting
153 was delayed, but not blocked, in *Tead1* cKO.
154 At P22, when WT SNs were fully myelinated, *Tead1* cKO SNs were largely
155 unmyelinated and exhibited areas of unsorted axon bundles, of sorted but unmyelinated axons,
156 and of thinly myelinated axons (Figure 2F, Figure 2-figure supplement 1A). Notably, at P50, this
157 phenotype was unchanged from that at P22: areas of unsorted bundles, promyelination, and thin
158 myelination persisted (Figure 2G, Figure 2-figure supplement 1A). TEM analysis confirmed that
159 myelin was indeed thinner in *Tead1* cKO than in WT at both P22 and P50 (Figure 2F, 2G, Figure
160 2-figure supplement 1B). The myelin thickness measured as g-ratio, i.e., the ratio between the
161 axon diameter and the fiber diameter (axon plus myelin sheath), did not significantly change in

162 cKO between P22 and P50 (Figure 2H), suggesting that growth of the myelin sheath relative to
163 axon diameter did not increase over this period. These data suggest that myelination in *Tead1*
164 cKO was arrested rather than delayed. Plots of g-ratio versus axon diameter showed that the
165 mutant defect was present in axons of all diameters but was particularly notable in those of larger
166 diameter (Figure 2I, 3J). The mean axon diameter was also reduced in cKO at P22, though it
167 increased with age (Figure 2K). Collectively, these data show that TEAD1 is required for timely
168 radial sorting, myelin formation and growth during development. Although some axons become
169 myelinated in *Tead1* cKO, their myelin sheaths fail to properly grow in proportion to axon
170 diameter in the absence of TEAD1.
171
172 **TEAD1 is required for proper formation of Remak bundles**
173 Remak bundle formation was also abnormal in *Tead1* cKO mice. In WT SNs at P22 and
174 P50, small diameter axons were present in Remak bundles, with each C-fiber ensheathed by SC
175 cytoplasm (Figure 2F, 2L). In *Tead1* cKO, C-fibers were also present in bundles in which axons
176 were rarely larger than 1 μm in diameter, suggesting that small diameter axons were almost fully
177 sorted. However, at both P22 and P50, the observed bundles were frequently small, often the size
178 of a large myelinated axon, and were occasionally thinly myelinated. Notably, a SC surrounded
179 each bundle but individual C-fibers of most Remak bundles were not ensheathed by SC
180 cytoplasm (Figure 2L). Quantification showed that ~80% of C-fibers were not ensheathed by SC
181 cytoplasm in P50 *Tead1* cKO SNs (Figure 2M). Thus, TEAD1 is required to develop proper
182 association of C-fibers with non-myelinating SCs in Remak bundles.
183
184 **TEAD1 regulates SC proliferation both positively and negatively to promote myelination**
185 For myelination and Remak bundle formation to occur properly, timely generation of
186 sufficient numbers of SCs is essential. To determine if the defects of myelination and Remak
187 bundles in *Tead1* cKO are due to defective SC proliferation, we counted SCs. At P3, SC number
188 in cKO SNs was about half that of WT (Figure 3A). Consistently, the number of SCs in the cell
189 cycle (Ki67-positive; Figure 3B) and in S-phase (EdU-positive; Figure 3C) was greatly reduced
190 in cKO at P3. Thus, TEAD1 is required for optimal SC proliferation during development.
191 Notably, at P22 and P50, SC numbers in cKO were markedly increased and became more
192 than twice those of WT (Figure 3A). As cKO SC numbers were similar at P22 and P50, we

193 reasoned that between P3 and P22, SC proliferation must occur at an abnormally high rate.
194 Indeed, the number of SCs that were Ki67-positive or EdU-positive was significantly increased
195 in cKO at P22 (Figure 3B, 3C). The increased SC numbers were not due to proliferation of
196 residual SCs that express TEAD1: TEAD1 was absent in most EdU-positive SCs in *Tead1* cKO
197 (Figure 3D). These data suggest that, during development, SCs switch from requiring TEAD1 for
198 optimal proliferation, to requiring TEAD1 for timely exit from the cell-cycle, which is a
199 prerequisite for SC differentiation and the onset of myelination (Hindley & Philpott, 2012).
200

201 **TEAD1 is required for Krox20 to upregulate myelin proteins, but not for Krox20**
202 **upregulation**

203 Our findings thus far show that, in the absence of TEAD1 in the SCs of *Tead1* cKO, most
204 axons are not myelinated, which grossly phenocopied *Yap1/Wwtr1* iDKO (*Yap1* and *Wwtr1*
205 encode the proteins commonly listed as YAP and TAZ, respectively). *Yap1/Wwtr1* cDKO
206 exhibited a complete failure of myelination due to arrest of their SCs as promyelinating SCs, in
207 part because they fail to upregulate Krox20/Egr2 (Early Growth Response 2), which drives
208 transcription of myelin proteins (Grove et al., 2017). To determine whether TEAD1 is required
209 for Krox20 upregulation, we first investigated Oct6 (Pou3f1, Scip), whose upregulation precedes
210 and is required for Krox20 upregulation; Oct6 is subsequently downregulated, possibly by
211 Krox20 in a feedback mechanism (Ryu et al., 2007; Zorick, Syroid, Brown, Gridley, & Lemke,
212 1999). Western blotting of P50 SN lysates showed minimal expression of Oct6 in WT, but
213 abnormally upregulated expression in *Tead1* cKO (Figure 4A). Immunohistochemistry of P50
214 cKO SNs also showed intense Oct6 expression in ~80% of SC nuclei; Oct6 expression was
215 minimal in WT (Figure 4B). Notably, at both P11 and P50, a similar percentage of SCs
216 expressed Krox20 in *Tead1* cKO, as in WT SNs (Figure 4C). In Western blots, Krox20 was
217 upregulated >4-fold in cKO compared to WT (Figure 4A). As adult *Tead1* cKO mice contain ~2-
218 fold more SCs than WT (Figure 3A), these data suggest that each SC in *Tead1* cKO contains ~2-
219 fold more Krox20 than WT. Thus, in contrast to SCs lacking YAP/TAZ, SCs lacking TEAD1
220 upregulate Krox20, suggesting that TEAD1 is dispensable for YAP/TAZ to upregulate Krox20.

221 Consistent with the idea that Krox20 is pivotal for myelin gene transcription, expression
222 of myelin basic protein (MBP), and myelin protein zero (MPZ), was abundant in WT P50 SNs
223 (Figure 4A). In contrast, despite ample expression of Krox20, both MBP and MPZ were

224 markedly decreased in *Tead1* cKO, indicating that Krox20 fails to properly upregulate myelin
225 proteins without TEAD1. To exclude the possibility that Krox20 expressed in cKO SCs is
226 defective, we took advantage of the earlier finding that loss of Krox20 or its co-factors, Nab1/2,
227 causes SCs to remain aberrantly in the cell-cycle (Le, Nagarajan, Wang, Svaren, et al., 2005;
228 Zorick et al., 1999). Therefore, we studied whether EdU-positive SCs in the cell-cycle of P11
229 cKO were also positive for Krox20, which would indicate defective Krox20. We found that,
230 although ~65% of SC nuclei contained Krox20, only a few EdU-positive SCs exhibited even
231 minimal Krox20 immunoreactivity in either WT or *Tead1* cKO (Figure 4D). Thus, despite high
232 levels of functional Krox20, myelin protein expression was greatly reduced in cKO SCs,
233 suggesting that TEAD1 is dispensable for Krox20 upregulation but required for Krox20 to
234 upregulate transcription of myelin proteins during development.
235
236 **TEAD1 and YAP/TAZ upregulate cholesterol biosynthetic enzymes, FDPS and IDI1**
237 Myelination of peripheral nerves by SCs requires a large amount of lipid and cholesterol
238 biosynthesis. De novo biosynthesis of fatty acids (integral building blocks of lipids) and
239 cholesterol is crucially important for SCs to initiate myelination and to grow a myelin sheath
240 (Montani et al., 2018; Norrmen et al., 2014; Saher et al., 2009; Verheijen et al., 2009). YAP/TAZ
241 may regulate these pathways, as suggested by reduced mRNA expression in *Yap1/Wwtr1* cDKO
242 of SREBPs TFs (Sterol regulatory element binding proteins) and their target enzymes involved
243 in lipid/cholesterol biosynthesis (Deng et al., 2017; Poitelon et al., 2016). We therefore
244 investigated, at the protein level, whether TEAD1 and YAP/TAZ are required for fatty acid
245 and/or cholesterol synthesis. To test this premise, we examined expression of SREBP1 and its
246 target SCD1 (Stearoyl-CoA desaturase-1), which upregulates fatty acid synthesis, and of
247 SREBP2 and its targets HMGCR (HMG-CoA reductase), FDPS (Farnesyl Diphosphate
248 Synthase) and IDI1 (Isopentenyl-diphosphate delta isomerase 1), which upregulate cholesterol
249 synthesis (Leblanc et al., 2005; Verheijen et al., 2009). Because SREBP pathways are
250 upregulated early postnatally for myelination in WT, their upregulation may simply be delayed
251 in developmentally delayed *Tead1* cKO. We therefore investigated SREBP pathways both at P8
252 and P40 in WT and *Tead1* cKO mice. Western blot analysis showed that levels of nuclear
253 SREBP1 were not affected by loss of TEAD1 at P8, and only slightly reduced at P40 (Figure
254 5A). SCD1 was reduced at P8, but slightly increased at P40. In contrast to SREBP1, SREBP2

255 was ~50% reduced in *Tead1* cKO at both P8 and P40. Despite marked reduction in SREBP2,
256 HMGCR was not reduced at P8 or P40. However, both FDPS and IDI1 levels were greatly
257 reduced at both P8 and P40 (Figure 5A).
258 It is possible that HMGCR was not reduced in cKO due to TEAD1 redundancy and
259 compensation by other TEADs. If so, then HMGCR levels should be reduced in *Yap1/Wwtr1*
260 cDKO, because YAP/TAZ are the primary partners for all TEADs (Holden & Cunningham,
261 2018; Zheng & Pan, 2019). To test this idea, we examined SREBP pathways in *Yap1/Wwtr1*
262 cDKO SNs at P60 because developmental delay is greater in *Yap1/Wwtr1* cDKO than in *Tead1*
263 cKO SNs (Grove et al., 2017). We found that, as in *Tead1* cKO, SREBP1 levels were unaffected
264 and SCD1 levels were markedly increased by the loss of YAP/TAZ in cDKO at P60 (Figure 5B).
265 Unlike in *Tead1* cKO, levels of SREBP2 were not markedly reduced in Yap1/Wwtr1 cDKO. As
266 in *Tead1* cKO, however, HMGCR levels were not reduced in Yap1/Wwtr1 cDKO, whereas
267 levels of FDPS and IDI1 were greatly reduced. These results therefore indicate that YAP/TAZ-
268 TEAD1 transcriptional complex selectively upregulates IDI1 and FDPS, contributing to
269 cholesterol biosynthesis. Together with the lack of synthesis of myelin proteins, this reduction in
270 cholesterol biosynthesis may prevent myelin formation and growth in *Tead1* cKO.
271
272 **TEAD1 is largely dispensable for myelin maintenance in adult Schwann cells**
273 Because TEAD1 is required for myelin formation and growth and Remak bundle
274 formation during development, we next investigated its role in maintenance and regeneration of
275 peripheral nerves in adults. We crossed *Tead1*$^{fl/fl}$ mice with mice carrying a tamoxifen-inducible
276 *Plp1*-CreER (Leone et al., 2003) to generate *Plp1* -CreER*; Tead1*$^{fl/fl}$ (hereafter *Tead1* iKO) and
277 inducibly inactivated SC *Tead1* in adult *Tead1* iKO mice. Western blotting showed markedly
278 reduced TEAD1 in *Tead1* iKO (Figure 6-figure supplement 1A). Residual TEAD1 is likely not
279 associated with SCs. Indeed, immunostaining of WT and induced iKO SNs consistently showed
280 that TEAD1 was deleted in >95% of SC nuclei in both intact and regenerating iKO SNs, whereas
281 TEAD1 was present in 100% of SC nuclei of WT SNs (Figure 6-figure supplement 1B, 1D). As
282 anticipated, iKO SC nuclei in both intact and regenerating nerves were strongly immunostained
283 by pan-TEAD antibody, presumably indicating the presence of other TEADs (Figure 6-figure
284 supplement 1C, 1E). We also found that YAP/TAZ were transcriptionally functional in adult SCs

285 lacking TEAD1, as indicated by strong nuclear expression of YAP/TAZ in SCs of both intact
286 and regenerated iKO SNs (Figure 6-figure supplement 1F, 1G).
287 *Tead1* iKO mice appeared normal without obvious signs of peripheral neuropathy up to 5
288 months post-tamoxifen, the longest time of observation (Figure 6A). TEM analysis of iKO SNs
289 between 3 to 5 months post-tamoxifen revealed, however, some large axons undergoing
290 demyelination or completely demyelinated, which were undetectable in WT SNs (Figure 6B).
291 The demyelinated axons were observed in discrete regions of SNs, indicating segmental
292 demyelination (<5% large axons on 12 TEM sections exhibiting demyelinated axons). NCV of
293 these iKO mice did not significantly differ from that of WT (Figure 6C). Therefore, loss of
294 TEAD1 in adult SCs evoked only modest focal demyelination in a small number of axons, which
295 did not cause significant functional impairment of peripheral nerves.
296
297 **TEAD1 is required for maintaining structural integrity of Remak bundles**
298 Next, we examined Remak bundles in *Tead1* iKO mice. As in WT SNs, C-fibers in WT
299 mice were individually ensheathed by SC cytoplasm. In stark contrast, in *Tead1* iKO, many C-
300 fibers in most Remak bundles were not ensheathed by SC cytoplasm (Figure 6D). Furthermore,
301 some small Remak bundles were occasionally myelinated (Figure 6E), as in *Tead1* cKO SNs.
302 Thus, TEAD1 is required for formation as well as maintenance of Remak bundles.
303
304 **TEAD1 is dispensable for YAP/TAZ to maintain Krox20, FDP, and IDI1 expression**
305 To investigate why the demyelinating phenotype of *Tead1* iKO is much milder than that
306 of *Yap1/Wwtr1* iDKO, we first investigated expression of Krox20, which is required for myelin
307 maintenance (Decker et al., 2006). We previously observed that Krox20 is markedly
308 downregulated in *Yap1/Wwtr1* iDKO SCs, which correlated with frequent segmental
309 demyelination and markedly reduced NCV (Grove et al., 2017). As a control, we injected *Plp1-*
310 *CreER; Yap1*$^{fl/fl}$*; Wwtr1*$^{fl/fl}$ mice with tamoxifen and reproduced our previous result: Krox20 was
311 dramatically downregulated in most *Yap1/Wwtr1* iDKO SCs only 2 weeks post-tamoxifen
312 (Figure 7A). In contrast, in *Tead1* iKO, Krox20 expression was indistinguishable from WT even
313 at 6 weeks post-tamoxifen (Figure 7B). We then investigated Oct6 expression. Unlike in
314 *Yap1/Wwtr1* iDKO SNs (Grove et al., 2017), Oct6 was not elevated in *Tead1* iKO SNs (Figure
315 7C). Thus, TEAD1 is dispensable for maintaining Krox20 expression in adult SCs.

316 Next, we investigated SREBP pathways, which are required for developmental
317 myelination (Saher et al., 2009; Verheijen et al., 2009). Whether these pathways are also
318 involved in myelin maintenance has not been studied. We first assessed the effects of acute loss
319 of YAP/TAZ on these pathways in adult SCs. Western blotting of WT and *Yap1/Wwtr1* iDKO
320 SN lysates showed that the SREBP1 pathway and expression of SREBP2 and HMGCR in the
321 SREBP2 pathway were unaffected in *Yap1/Wwtr1* iDKO (Figure 7D). However, FDPS and IDI1
322 levels were significantly downregulated in *Yap1/Wwtr1* iDKO, recapitulating the effect of
323 developmental loss of YAP/TAZ on these proteins (Figure 5B). Thus, the acute downregulation
324 of these key enzymes for cholesterol biosynthesis correlates with the acute demyelination
325 previously observed in *Yap1/Wwtr1* iDKO mice. This result suggests that YAP/TAZ maintain
326 myelination through both myelin gene expression and the cholesterol biosynthesis pathway.
327 Western blotting of *Tead1* iKO SN lysates revealed that the SREBP pathways were not
328 significantly affected by loss of TEAD1 (Figure 7E), unlike *Tead1* cKO in which FDPS and IDI1
329 were markedly downregulated (Figure 5A). This result suggests that TEAD1 is dispensable for
330 cholesterol synthesis in adult SCs.
331
332 **TEAD1 is absolutely required for myelination of regenerating axons after nerve injury**.
333 Next, we investigated whether TEAD1 is required for axon regeneration and
334 remyelination after nerve injury. YAP/TAZ are not required for axon regeneration but are crucial
335 for remyelination (Grove et al., 2017; Jeanette et al., 2021). Because *Yap1/Wwtr1* iDKO mice die
336 ~2 weeks post-injury (wpi), it remains possible that remyelination is delayed rather than
337 completely blocked. In contrast, *Tead1* iKO mice are not susceptible to early death. We,
338 therefore, examined them 4 weeks after crushing SN (Figure 8A), when hindlimb muscles are
339 fully reinnervated in WT. We first verified efficient deletion of TEAD1 in >95% SCs of *Tead1*
340 iKO mice after nerve crush (Figure 6-figure supplement 1D). Longitudinal sections of iKO SNs
341 showed numerous Tuj1-labeled axons that regenerated along the distal nerve stump, as in WT
342 SNs (Figure 8B). However, MBP immunoreactivity was greatly reduced in the distal nerve
343 stump of *Tead1* iKO, compared to WT, suggesting that axons regenerated but were not
344 remyelinated. We also found that regenerated axons reached hindlimb muscles and reinnervated
345 neuromuscular junctions (NMJs) in iKO, as in WT (Figure 8C). Moreover, *Tead1* iKO
346 frequently exhibited features of paralyzed muscles, such as axon terminals that grew past the

347 synaptic area, fragmented clusters of acetylcholine receptors (AChRs), and satellite extra-
348 synaptic AChRs (Wright, Cho, & Son, 2007). Semithin and EM analysis confirmed virtual
349 absence of myelinated axons in iKO SNs; although large axons were associated with SCs, they
350 were not myelinated (Figure 8D). Accordingly, electrical stimulation of iKO SNs did not elicit
351 CMAPs or NCV (Figure 8E). Thus, like YAP/TAZ, TEAD1 in SCs is not required for axon
352 regeneration but is required for remyelination after nerve injury.
353 After injury, SCs transdifferentiate into growth-promoting repair SCs, which proliferate
354 and reach a peak around 3 days post-injury (dpi) (Clemence, Mirsky, & Jessen, 1989; Jessen &
355 Mirsky, 2016; Tricaud & Park, 2017). Quantitative analysis of SC proliferation at 3 dpi by
356 counting $EdU^+/Sox10^+$ SCs showed that a similar percentage of SCs were in S-phase in both WT
357 and *Tead1* iKO SNs (Figure 8F), suggesting that, like YAP/TAZ (Grove et al., 2017), TEAD1 is
358 not required for proliferation of repair SCs. Lastly, we counted $Krox20^+$ and $Oct6^+$ SCs at 4 wpi.
359 Notably, in contrast to *Yap1/Wwtr1* iDKO SCs, which fail to upregulate Krox20 after injury
360 (Grove et al., 2017), Krox20 was upregulated in *Tead1* iKO SCs, as in WT SCs (Figure 8G).
361 Furthermore, Oct6 was aberrantly elevated in *Tead1* iKO SCs, like in *Tead1* cKO SCs during
362 development (Figure 8H). These results suggest that, similar to developmental myelination,
363 remyelination requires TEAD1 for Oct6 downregulation and for Krox20 to upregulate myelin
364 proteins. Additionally, almost complete absence of remyelination at 4 wpi highlights the non-
365 redundant, crucial role of TEAD1 in the remyelination of regenerating nerves after injury.
366

367 **DISCUSSION**

368 The present study conclusively establishes TEAD1 as a crucial TF mediating myelin formation,
369 growth, and regeneration. TEAD1 promotes myelination by dually regulating SC proliferation,
370 by enabling induced Krox20 to upregulate myelin proteins, and by upregulating cholesterol
371 biosynthetic enzymes. Our findings also suggest that TEAD1 is critical in the proper formation
372 and maintenance of Remak bundles.
373

374 **Unique, redundant, and opposing roles of TEAD1**

375 Although SCs express other TEADs, *Tead1* cKO mice grossly phenocopy *Yap1/Wwtr1* cDKO
376 mice. They exhibit abnormal SC proliferation, delayed radial sorting, blocked myelin formation
377 and remyelination, and normal axon regeneration. Furthermore, *Tead1* cKO mice, like

378 *Yap1/Wwtr1* cDKO, are defective in regulating Oct6, Krox20, myelin proteins, and enzymes that
379 synthesize cholesterol. These similarities show that YAP/TAZ regulate both SC proliferation and
380 differentiation, the two opposing processes crucial for myelination, by partnering mainly with
381 TEAD1 for developmental myelination and remyelination after injury. We also observed
382 multiple differences between *Tead1* cKO and *Yap1/Wwtr1* cDKO mice. Unlike *Yap1/Wwtr1*
383 cDKO, *Tead1* cKO initiates myelin formation in some developing axons and maintains
384 myelination in almost all adult axons. Additionally, in *Tead1* cKO, Krox20 is upregulated and a
385 large excess of SCs is generated. It is also notable that, whereas some developing axons are
386 myelinated in *Tead1* cKO, almost all axons regenerating after injury are unmyelinated. These
387 differences are likely due to stage-dependent redundancy and opposing roles of TEADs.
388 Consistent with this notion, loss of TEAD1 does not affect nuclear localization of YAP/TAZ,
389 which depends on interactions with TEADs (Diepenbruck et al., 2014; J. Kim et al., 2020; Kofler
390 et al., 2018; Yao et al., 2018). TEAD1-4 are all co-expressed in SCs through multiple stages of
391 nerve development, maintenance, and regeneration (Fernando et al., 2016; Grove et al., 2017; X.
392 He et al., 2018). Notably, nuclear retention of YAP/TAZ occurs in *Tead1* cKO and iKO SCs
393 when TEAD1 has a unique role in SCs for developmental myelination and remyelination. Thus,
394 other TEADs can retain nuclear YAP/TAZ, thereby supporting transcriptional activity of
395 YAP/TAZ, but cannot substitute for some or most of the functions of TEAD1 in a stage-
396 dependent manner.
397
398 It is also notable that, like YAP/TAZ, the unique roles of TEAD1 change dynamically in
399 successive steps of myelination, even though other TEADs are present. Thus, TEAD1 is
400 uniquely required for timely proliferation of SCs; uniquely opposes SC proliferation to promote
401 cell-cycle exit after radial sorting; redundantly promotes upregulation of Krox20; and then
402 uniquely promotes upregulation of myelin proteins and cholesterol biosynthetic enzymes. Such
403 unique and redundant roles for TEAD1 in the presence of other TEADs are supported by cell-
404 based transcription assays, in which YAP-TEAD4 can substitute for YAP-TEAD1 in
405 upregulating transcription from the Krox20 promoter, but not from the MPZ intronic enhancer
406 (Fernando et al., 2016). Stage-dependent function of TEADs was also reported in cortical
407 development, another multi-step differentiation program. As in nerve development, multiple
408 TEADs (TEAD1-3) are co-expressed throughout cortical development. Depending on the

409 differentiation stage, TEAD1 uniquely promotes proliferation, redundantly promotes
410 proliferation with TEAD2 and 3, or redundantly promotes differentiation with TEAD3, when it
411 is opposed by TEAD2 (Mukhtar et al., 2020).
412
413 As *Yap1/Wwtr1* cDKO SCs arrest at the promyelination stage, we were unable to investigate the
414 role of YAP/TAZ in myelin growth (Grove et al., 2017). In contrast, some *Tead1* cKO SCs can
415 myelinate but fail to grow myelin sheaths proportional in size to axon diameter. Importantly,
416 such myelinating SCs apparently lack TEAD1 because TEAD1 deletion is highly efficient in
417 *Tead1* cKO mice. Support for a role of TEADs in the regulation of myelin sheath thickness
418 comes from a study of TEAD4 cKO mice, in which SCs lacking TEAD4 gradually upregulate
419 myelin protein expression, resulting in adult mice with abnormally thick myelin (X. He et al.,
420 2018). Thus, it is possible that TEADs 1 and 4 oppose each other in the regulation of myelin
421 sheath growth. Likewise, they may oppose each other in the regulation of SC proliferation during
422 development, resulting in a large excess of SCs at P22 and P50 in *Tead1* cKO.
423
424 **TEAD1 regulation of Krox20 and myelin gene expression**
425 Previous work suggests that YAP/TAZ-TEAD1 promote myelination in part through direct
426 upregulation of Krox20 (Deng et al., 2017; Grove et al., 2017). Unlike *Yap1/Wwtr1* cKO mice,
427 *Tead1* cKO mice upregulate Egr2/Krox20, but they fail to upregulate myelin proteins and
428 cholesterol biosynthetic enzymes. Our findings extend previous work to suggest that TEAD1
429 functions redundantly in direct upregulation of Krox20, but that its function is required for
430 upregulated Krox20 to promote myelination. Krox20 activity may be repressed in *Tead1* cKO by
431 Oct6, which remains abnormally elevated. In support of this possibility, persistently elevated
432 Oct6 overrides Krox20 to inhibit myelin gene expression (Monuki, Kuhn, & Lemke, 1993; Ryu
433 et al., 2007). Other mice with defective lipid biosynthesis and a phenotype like *Tead1* cKO also
434 have abnormally elevated Oct6 after Krox20 upregulation (Norrmen et al., 2014; Sherman et al.,
435 2012). An alternative possibility is that a transcriptional co-activator that synergizes with Krox20
436 is absent in *Tead1* cKO SCs. We speculate that TEAD1 itself may function as such a factor.
437 Supporting this idea are reports that gene regulatory elements function by co-binding several
438 TFs, which synergistically activate transcription (Heinz, Romanoski, Benner, & Glass, 2015;
439 Ren & Yue, 2015), as at the Krox20 MSE (Myelinating Schwann cell element) which is the

440 enhancer responsible for Krox20 expression (Ghislain & Charnay, 2006; Grove et al., 2017; Y.
441 He et al., 2010; Kao et al., 2009). Krox20 synergizes with Sox10 to activate myelin genes (Jones
442 et al., 2007) and with SREBP to activate lipid biosynthesis genes (Leblanc et al., 2005). Like
443 Krox20, TEAD1 can directly promote transcription from PMP22 and MPZ myelin gene
444 enhancers (Fernando et al., 2016; Lopez-Anido et al., 2016). Alternatively, or additionally,
445 TEAD1 may function indirectly by upregulating co-factors, such as SREBP2, which is reduced
446 in *Tead1* cKO. Notably, lipid biosynthesis is necessary to downregulate Oct6 and upregulate
447 myelin gene transcription during developmental myelination (Saher et al., 2009; Verheijen et al.,
448 2009). An interesting possibility, therefore, is that YAP/TAZ-TEAD1 and Krox20 may
449 cooperatively downregulate Oct6 and upregulate myelin gene expression in part by promoting
450 lipid biosynthesis.
451
452 **YAP/TAZ-TEAD1 regulation of cholesterol biosynthesis**
453 SREBP1 levels are not altered in *Tead1* cKO or *Yap1/Wwtr1* cDKO, suggesting that fatty acid
454 synthesis is not directly regulated by TEAD1 or YAP/TAZ. It is likely that the reduced levels of
455 SCD1 at P8 and slight increase at P40 in *Tead1* cKO, and the large increase in SCD1 in
456 *Yap1/Wwtr1* cDKO at P60 are due to developmental delay in these mutants. We did not observe
457 downregulation of HMGCR in *Tead1* cKO or *Yap1/Wwtr1* cDKO mice at P8 or P40, which
458 contradicts the report of reduced mRNA expression of HMGCR in *Yap1/Wwtr1* mutants at P3
459 and P5 (Deng et al., 2017; Poitelon et al., 2016); we suggest this difference is due to
460 developmental delay in *Tead1* cKO and *Yap1/Wwtr1* cDKO. However, marked downregulation
461 of IDI1 and FDPS in *Tead1* cKO, *Yap1/Wwtr1* cDKO, and *Yap1/Wwtr1* iDKO suggests that
462 cholesterol biosynthesis is defective in these mutants. In support of this notion, SC-selective
463 deletion of SCAP (SREBP cleavage activation protein), which is required to produce active
464 SREBP1 and SREBP2 (Verheijen et al., 2009), or of Squalene synthase, an essential enzyme in
465 cholesterol biosynthesis (Saher et al., 2009), evokes phenotypes which are remarkably similar to
466 those of *Tead1* cKO mice: both mutants have an increased number of SCs, a severe delay at the
467 promyelination stage, and persistently thin myelin. In addition, in SCAP cKO, Oct6 is
468 upregulated continuously and Squalene synthase cKO fails to upregulate myelin gene
469 transcription, resulting in severely reduced MBP, MPZ, and PMP22 protein levels.
470

471 How might YAP/TAZ-TEAD1 regulate IDI1 and FDPS? Multiple studies show that YAP/TAZ
472 can activate the mTORC1 pathway (Hu et al., 2017; M. Kim, Kim, Johnson, & Lim, 2015), and
473 that IDI1 and FDPS levels are reduced in SNs of Raptor cKO, a core component of mTORC1
474 (Norrmen et al., 2014). Furthermore, the Raptor cKO phenotype is like that of *Tead1* cKO,
475 exhibiting an increased number of SCs, normal upregulation of Krox20, persistent upregulation
476 of Oct6, delay at the promyelination stage, and thin myelin. However, HMGCR protein levels
477 are reduced, and aberrant upregulation of Oct6 is transient (Norrmen et al., 2014). After nerve
478 injury, formation of repair SCs is delayed in Raptor mutants (Norrmén et al., 2018), unlike
479 TEAD1 and YAP/TAZ mutants. These differences suggest that YAP/TAZ-TEAD1 are not
480 directly upstream of mTORC1. Another possibility is that YAP/TAZ-TEAD1 may directly
481 regulate transcription of IDI1 and FDPS genes. Such direct regulation of cholesterol biosynthetic
482 enzymes has been observed for other TFs in SCs (M. Kim et al., 2018; Leblanc et al., 2005).
483
484 **TEAD1 regulation of Remak bundles**
485 In both *Tead1* cKO and iKO mice, there is defective ensheathment of C-fibers by non-
486 myelinating SCs in Remak bundles. This phenotype is distinct from those mutants in which SCs
487 surround and occasionally myelinate bundles filled with large and small caliber axons, which are
488 considered radial sorting defects (Feltri, Poitelon, & Previtali, 2016). Remak bundles are
489 occasionally myelinated in WT SNs during early postnatal development, but this defect is
490 corrected and does not persist in adults (Rasi et al., 2010). Thus, the defective Remak bundles
491 that we observed in *Tead1* cKO are not due to developmental delay.
492
493 Remak bundles form normally at P60 in *Yap1/Wwtr1* cDKO, although many large bundles
494 containing mixed caliber axons are present during development (Grove et al., 2017). The
495 difference between *Tead1* and *Yap1/Wwtr1* mutants is supported by the presence of TEAD1 and
496 absence of YAP/TAZ in non-myelinating SC nuclei (Grove et al., 2017). Notably, defective SC
497 ensheathment of C-fibers is observed in various SC developmental mutants, including those with
498 defective SC basal lamina (Rasi et al., 2010) and overexpression of NRG1-IIIb (Neuregulin 1
499 type-IIIb) in axons (Gomez-Sanchez et al., 2009). Therefore, it is possible that TEAD1 mediates
500 extracellular signaling from the SC basal lamina and/or axons that is responsible for forming and
501 maintaining proper association of SCs with C-fibers. Notably, SC ensheathment of C-fibers is

502 required for normal NCV (Taveggia et al., 2005), and NCV in the mutants overexpressing
503 NRG1-IIIb is significantly reduced compared to WT (Gomez-Sanchez et al., 2009). Future
504 studies will address NRG1 signaling and NCV in cKO and iKO mice lacking TEAD1 and/or
505 other TEADs.
506
507 **MATERIALS AND METHODS**
508

Reagent type (species) or resource	Designation	Source or Reference	Identifiers	Additional Information
Strain, strain background (*Mus musculus*)	C57Bl/6	Jackson Laboratory	Stock #: 000664; RRID:IMSR JAX:000664	
Genetic reagent (*M. musculus*)	*Plp1*-Cre-ERT2		MGI:2663093	(Leone et al., 2003)
Antibody	anti-Yap/Taz (rabbit monoclonal)	Cell Signaling Technology	D24E4, #8418 RRID:AB_10950494	IHC 1:200 Western 1:1000
Antibody	anti-SCG10 (rabbit monoclonal)	Novus Biologicals	NBP1-49461 RRID:AB_10011569	IHC 1:5000
Antibody	anti-Yap (rabbit monoclonal)	Cell Signaling Technology	D8H1X, #14074 RRID:AB_2650491	IHC 1:200
Antibody	anti-Sox10 (goat polyclonal)	R&D Systems	#AF-2864 RRID:AB_442208	IHC 1:100
Antibody	anti-Sox10 (rabbit monoclonal)	Abcam	EPR4007, #ab155279 RRID:AB_2650603	IHC 1:250
Antibody	anti-Egr2 (rabbit polyclonal)	Professor Dies Meijer, University of Edinburgh		IHC 1:4000
Antibody	anti-Oct6 (rabbit monoclonal)	Abcam	EP5421, #ab126746 RRID:AB_11130256	WB 1:1000

Antibody	anti-Oct6 (rabbit polyclonal)	Abcam	#ab31766 RRID:AB_776899	IHC 1:800
Antibody	anti-c-Jun (mouse monoclonal)	BD Transduction Laboratories	#610326 RRID:AB_397716	IHC 1:500
Antibody	anti-c-Jun (rabbit monoclonal)	Cell Signaling Technology	60A8, #9165 RRID:AB_2130165	WB 1:1000
Antibody	anti-pS63-c-Jun (rabbit polyclonal)	Cell Signaling Technology	#9261 RRID:AB_2130162	IHC 1:100
Antibody	anti-Ki67 (rabbit polyclonal)	Abcam	#ab15580 RRID:AB_443209	IHC 1:200
Antibody	anti-p75NGFR (goat polyclonal)	Neuromics	#GT15057 RRID:AB_2737189	IHC 1:400
Antibody	anti-Tubulin β3 (rabbit polyclonal)	Biolegend	#802001 RRID:AB_2564645	IHC 1:1000
Antibody	IRDye-680 (goat anti-mouse)	LI-COR	#926-32220 RRID:AB_621840	WB 1:15,000
Antibody	HRP-Goat anti-mouse secondary antibody	Jackson Immunoresearch	#715-035-150 RRID:AB_2340770	WB 1:12,000
Antibody	HRP-Goat anti-rabbit secondary antibody	Jackson Immunoresearch	#115-055-062 RRID:AB_2338533	WB 1:12,000
Chemical compound, drug	Araldite 6005	EMS	#10920	
Chemical compound, drug	DDSA	EMS	#13710	
Chemical compound, drug	DBP	EMS	#13101	
Chemical compound, drug	BDMA	EMS	#11400-25	
other	Coated grids (100 mesh)	EMS	#FF100-Cu	
Chemical compound, drug	Osmium tetroxide (4% solution)	EMS	#19170	

Chemical compound, drug	Lead nitrate	EMS	#17900	
Chemical compound, drug	Sodium citrate	EMS	#21140	
Chemical compound, drug	Uranyl acetate	EMS	#22400	
Chemical compound, drug	Sodium borate	EMS	#21130	
Chemical compound, drug	Toluidine blue	EMS	#22050	
Chemical compound, drug	Paraformaldehyde	Sigma-Aldrich	#158127	
Commercial assay or kit	Click-It EdU Alexa Fluor 594 kit	ThermoFisher Scientific	#C10339	
Chemical compound, drug	EdU	ThermoFisher Scientific	#E10187	
Chemical compound, drug	Tamoxifen	Sigma-Aldrich	#T5648	
other	DAPI stain	Invitrogen	#D1306	IHC 1:250
Antibody	Alexa 488, 568 or 647 secondaries	Jackson Immunoresearch		IHC 1:250 to 1:1000
software, algorithm	Image Studio Lite	LI-COR, Inc		
software, algorithm	Prism	GraphPad Software, Inc		
software, algorithm	Stata	StataCorp LP		Mann-Whitney test

509

510 **Animals**

511 All surgical procedures and animal maintenance complied with the National Institute of Health
512 guidelines regarding the care and use of experimental animals and were approved by the

513 Institutional Animal Care and Use Committee (Protocol# 4920) of Temple University,
514 Philadelphia, PA, USA. Generation and genotyping of mice carrying targeted loxP sites in the
515 *Tead1* gene have been described previously (Wen et al., 2017). Targeted ablation of *Tead1* in
516 Schwann cells of embryonic mice was achieved by crossing *Tead1*$^{fl/fl}$ mice with mice transgenic
517 for *Cre* driven by the *Mpz* promoter (*Tead1* cKO mice). Targeted ablation of *Tead1* in Schwann
518 cells of adult mice was by crossing *Tead1*$^{fl/fl}$ mice with mice transgenic for the inducible Cre
519 recombinase *Cre-ERT2* under control of the *Plp1* promoter (*Tead1* iKO mice). Control mice
520 contained floxed *Tead1* alleles but were not transgenic for *Cre* or *Cre-ERT2*. *Mpz-cre*;*Yap1*$^{fl/fl}$;
521 *Wwtr1*$^{fl/fl}$ (*Yap1/Wwtr1* cDKO) and *Plp1-creERT2*; *Yap1*$^{fl/fl}$; *Wwtr1*$^{fl/fl}$ (*Yap1/Wwtr1* iDKO) mice
522 used in this study were generated and genotyped as described previously (Grove et al., 2017).
523 Both male and female mice were used in all experiments and were maintained on the C57BL/6
524 background.
525
526 **Tamoxifen administration**
527 Tamoxifen was prepared and injected into 6–8-week-old *Tead1* or *Yap1/Wwtr1* mutant mice as
528 previously described (Grove et al., 2017). A 10 mg/ml solution of tamoxifen was made in 10:1
529 sunflower oil: 100% ethanol. This solution was injected intraperoneally at a concentration of 0.2
530 mg/g body weight. Injection was once daily for 5 days, followed by a 2-day break, then once
531 daily for 5 consecutive days.
532
533 **Nerve crush**
534 Sciatic nerves of right hindlimbs were crushed 24 h after the final tamoxifen injection, as
535 described previously (Grove et al., 2020; Son & Thompson, 1995). A small skin incision was
536 made in the posterior thigh and calf of the animals anesthetized by isoflurane. The sciatic nerve
537 was crushed with a fine forceps (#5) for 10 seconds (3X) adjacent to the sciatic notch. The crush
538 site was marked using charcoal-coated forceps, and the wound was closed. To identify
539 proliferating Schwann cells, we intraperitoneally injected EdU (80 μg/g) eighty minutes before
540 euthanasia, as previously described (Grove et al., 2017).
541
542 **Western blotting**

543 After removal of epineurium and perineurium, sciatic nerves were snap-frozen in liquid nitrogen
544 and stored at -80ºC. For Western blotting, sciatic nerves were lysed in RIPA buffer (25 mM Tris
545 pH 7.5, 150 mM NaCl, 1% Triton X-100, 0.5% sodium deoxycholate, 1 mM EDTA, 0.1% SDS);
546 for immunoprecipitation, lysis was in co-IP buffer (50 mM Tris pH 8.0, 150 mM NaCl, 0.5%
547 Triton X-100, 10% glycerol, 1 mM EDTA), both containing protease and phosphatase inhibitors.
548 Lysis was for 40 minutes on ice, followed by microcentrifugation at 14,000 rpm for 20 minutes.
549 Protein concentration was determined using the BCA assay (ThermoFisher).
550 Primary antibodies were used at the following concentrations for Western blots: rabbit
551 anti-Krox20 (Covance; 1:400), rabbit anti-Oct6 (Abcam ab126746; 1:1000), mouse anti-Myelin
552 Basic Protein (Covance SMI94; 1:1000), mouse anti-beta actin (SIGMA-Aldrich A5441;
553 1:5000), rabbit anti-TEAD1 (Cell Signaling D9X2L, #12292; 1:1000), rabbit anti-TEAD2
554 (Novus Biologicals, #NBP3-05267; 1:1000), rabbit anti-TEAD3 (Cell Signaling #13224;
555 1:1000), rabbit anti-TEAD4 (Santa Cruz, #sc-101184; 1:1000), rabbit anti-pan-TEAD (Cell
556 Signaling, #13295; 1:1000), rabbit anti-YAP/TAZ (Cell Signaling D24E4, #8418; 1:1000, 1:100
557 for immunoprecipitations), rabbit anti-phospho-YAP(Ser127) (Cell Signaling D9W2I #13008;
558 1:1000), rabbit anti-phospho-YAP(Ser397) (Cell Signaling D1E7Y #13619; 1:1000), rabbit-anti-
559 MPZ (Cell Signaling #57518; 1:1000), mouse anti-SREBP1 (Novus Biologicals, #NB600-582;
560 1:1000), rabbit anti-SCD1 (Cell Signaling, #2794; 1:1000), rabbit anti-SREBP2 (Bethyl
561 laboratories, #A303-125A), rabbit anti-HMGCR (Novus Biologicals, #NBP2-66888; 1:1000),
562 rabbit anti-FDPS (Proteintech, #16129-1-AP; 1:1000), rabbit anti-IDI1 (Proteintech, #11166-2-
563 AP; 1:1000). Control whole rabbit IgG for immunoprecipitations was from Jackson Laboratories
564 (011-000-003) and was used at 1μg/ml, which was several-fold greater than all other antibodies
565 used for immunoprecipitations. Secondary antibodies for Western blotting were HRP-linked
566 sheep anti-mouse IgG and donkey anti-rabbit (both GE Healthcare; 1:5000) and HRP-linked
567 mouse anti-rabbit, light-chain specific (Jackson ImmunoResearch 211-032-171; 1:20,000). Blots
568 were developed using ECL, ECL Plus (GE Healthcare) or Odyssey (LiCor).
569
570 **Immunohistochemistry, confocal and widefield fluorescence microscopy**
571 For immunostaining, sciatic nerves were removed and immediately fixed in 4%
572 paraformaldehyde in PBS for 1 hr. on ice. Nerves were washed 3 times in PBS, then stored in
573 15% sucrose in PBS overnight at 4°C for cryoprotection. Nerves were frozen-embedded in

574 cryoprotectant medium (Thermo Fisher Scientific, Waltham, MA) in isomethylbutane at -80°C.
575 7-10 μm sections from the nerves were cut using a cryostat (Leica Microsystems, Germany) and
576 collected directly onto glass slides. For immunolabeling, nerve sections were rehydrated in PBS,
577 permeabilized in 0.5% Triton/PBS for 20 min, washed with PBS, then blocked in 2% bovine
578 serum albumin (BSA) in PBS for 1 hr. Sections were incubated with primary antibodies in
579 blocking buffer overnight at 4°C in a hydrated chamber, washed with PBS, and incubated with
580 secondary antibodies in blocking buffer for 2 hrs. at room temperature. Sections were washed
581 with PBS, stained with DAPI for 10 min, and mounted with Vectashield mounting medium
582 (Vector Labs, Burlingame, CA).
583 Primary antibodies were used at the following concentrations for immunostaining of
584 cryosections: guinea pig anti-Sox10 (kind gift from Michael Wegner, University of Erlangen,
585 Bavaria, Germany; 1:1000), rabbit anti-Krox20 (Covance; 1:400), rabbit anti-Oct6 (Abcam
586 ab31766; 1:800), rabbit anti-Ki67 (Novocastra NCL-Ki67p; 1:200), rabbit anti-Neurofilament
587 200 (SIGMA-Aldrich N4142; 1:500), mouse anti-Neurofilament (Covance SMI 312; 1:1000),
588 mouse anti-Tubulin β3 (clone Tuj1, Covance #MMS-435P; 1:1000), mouse anti-SV2
589 (Developmental Studies Hybridoma Bank, Iowa; 1:10), rabbit anti-S100 (DAKO; 1:600), mouse
590 anti-Myelin Basic Protein (Covance SMI 94; 1:2000), rabbit anti-TEAD1 (Cell Signaling
591 D9X2L, #12292; 1:200), rabbit anti-pan-TEAD (Cell Signaling D3F7L, #13295; 1:200), rabbit
592 anti-YAP/TAZ (Cell Signaling D24E4, #8418; 1:200).
593 For immunostaining of extensor digitorum longus (EDL) and soleus muscles, mice were
594 perfused with 4% paraformaldehyde, and the muscles removed and post-fixed for 20 mins at
595 room temperature. Muscles were then incubated for 15 minutes with rhodamine-conjugated α-
596 bungarotoxin (Invitrogen, Carlsbad, CA), permeabilized in −20°C methanol for 5 min, and
597 blocked for 1 hr. in PBS containing 0.2% Triton and 2% BSA. The muscles were subsequently
598 incubated overnight at 4ºC in a cocktail of primary antibodies diluted in the blocking solution.
599 Axons and nerve terminals were labeled with mouse monoclonal antibodies to neurofilaments
600 (SMI 312; Sternberger Monoclonals, Baltimore, MD) and to a synaptic vesicle protein, SV2
601 (Developmental Studies Hybridoma Bank, Iowa City, IA). Schwann cells were labeled with
602 rabbit anti-cow S-100 polyclonal antibody (Dako, Carpentaria, CA). After incubation with the
603 primary antibodies, muscles were rinsed in PBS and incubated with secondary antibodies in the
604 blocking solution, for 1 hr. at room temperature. The muscles were then rinsed in PBS and

605 prepped for whole-mount by peeling the top layer of muscle fibers using microscissors and
606 forceps, as previously described (Son & Thompson, 1995). The resulting "muscle fillets" were
607 mounted on a slide and coverslipped.
608 Conventional fluorescence microscopy was performed using Olympus BX53 and Zeiss
609 Axio Imager 2 microscopes. Images were captured using Hamamatsu ORCA R2 C10600 or
610 Zeiss Axiocam HRm Rev 3 digital cameras, respectively, and Metamorph software. For confocal
611 microscopy, we used a Leica SP8 confocal microscope, with either a 40x 1.3 NA or 63x 1.4 NA
612 objective and Leica proprietary software. Acquired stacks were assembled using the maximum
613 projection tool, and figures were prepared using Adobe Photoshop.
614
615 **Electron microscopy, histology, and morphometry**
616 Mice were perfused intravascularly with 2.5% glutaraldehyde and 4% paraformaldehyde in 0.1M
617 cacodylate buffer pH 7.4. Sciatic nerves were removed and incubated in the same buffer for 90
618 min. at room temperature, then overnight at 4ºC. Specimens were post-fixed for 1 hr. with OsO_4,
619 dehydrated, then embedded in araldite. Semi-thin (0.5 μm) and ultrathin (70 nm) sections were
620 cut using an ultramicrotome and stained with toluidine blue or uranyl acetate and lead citrate,
621 respectively. Semi-thin sections were examined using bright field on an Olympus BX53
622 microscope, and images were captured using Hamamatsu ORCA R2 C10600 digital camera and
623 Metamorph software. For analysis of the number of myelin profiles in control vs mutant sciatic
624 nerves, semi-thin sections from proximal-, mid- and distal regions of the sciatic nerve were
625 taken, and 2 non- overlapping images of each section were obtained using the 60x objective. For
626 electron microscopy, stained ultrathin sections were examined using a JEOL 1010 electron
627 microscope fitted with a Hamamatsu digital camera and AMT Advantage image capture
628 software.
629
630 **Proliferation assays**
631 The percentage of Schwann cells in S-phase was measured by EdU incorporation. Mice were
632 injected intraperitoneally and subcutaneously with 80 μg/ g body weight of EdU dissolved in
633 PBS. Eighty min. later, mice were sacrificed, and sciatic nerves removed and fixed for 1 hr. in
634 4% paraformaldehyde; longitudinal 7μm cryosections were used for analysis. EdU incorporation
635 was identified using the Click-iT EdU Alexa Fluor 555 labeling kit (Molecular Probes); the

636 recommended protocol was followed, and labeling was for 1 hr. After EdU labeling, sections
637 were immunostained with anti-Sox10 to identify Schwann cells. The percentage of Schwann
638 cells (Sox10+ nuclei) that were EdU+ was determined by counting confocal images using
639 ImageJ software.
640
641 **Electrophysiology**
642 The procedure for measuring nerve conduction velocity was an adaption of a previously used
643 protocol (Schulz, Walther, Morrison, & Bauer, 2014). Mice were deeply anesthetized, and hair
644 was completely removed from the hindquarters. A 27g percutaneous needle electrode was
645 inserted subcutaneously over the femur to stimulate the sciatic nerve at two locations: at the hip
646 joint and 1cm distal to this site. The stimulation reference electrode (26G percutaneous needle)
647 was inserted over the back. Bipolar EMG electrodes were inserted subcutaneously in the digital
648 interosseous muscles to record compound action potentials in response to activation of the sciatic
649 nerve. Stimulation and recording were conducted on both hindlimbs. The muscle response was
650 first tested with single pulses (100 μs duration) to determine the threshold and level of activation
651 producing a stable compound action potential in the muscle. The level of stimulation which
652 produced stable responses was then used for two series of stimulations with 2-20s long trains of
653 biphasic square wave pulses (100 μs duration) delivered at 1-5 Hz. The nerve was rested for 2
654 min. between runs. Stimulation was delivered via an isolated pulse stimulator (A-M Systems
655 Model 2100, A-M Systems Inc, Carlsborg, WA). EMG compound muscle action potential
656 (CMAP) responses were recorded with a differential AC amplifier (A-M Systems Model 1700;
657 gain 1k-10k; pass band 10-50 KHz). Data was sampled at 50 KHz using LabVIEW (National
658 Instruments Corporation, Austin, TX) running on a personal computer. Multiple recordings were
659 taken at each location to ensure a minimum of 10 representative responses for each location and
660 animal. Electrophysiological data were analyzed using Igor Pro (Wavemetrics Inc, Lake
661 Oswego, OR).
662
663 **Data Analysis**
664 In each experiment, data collection and analysis were performed identically, regardless of mouse
665 genotype. We used the sample (replicate) size (number) typically used in earlier studies of
666 peripheral myelination. Data are presented as mean +/- SD. Statistical analysis was done using

667 Student's unpaired t-test for two-group comparisons and analysis of variance (ANOVA) with
668 Tukey's test for multiple comparisons, according to the number of samples and the analysis of
669 mice at multiple ages. Normal distribution of all data was tested using Shapiro-Wilk normality
670 test. Sample sizes were similar to those conventional in the field and are indicated in the main
671 text, methods, or figure legends. A p-value of 0.05 or less was considered statistically significant.
672

673 **ACKNOWLEDGMENTS**

674 We thank Alan Tessler and members of the Son laboratory for critical reading of the manuscript.
675 We thank Dr. Eric Olson for *Yap1* and *Wwtr1* floxed mice, Drs. Ueli Suter and Kelly Monk for
676 *Plp1*-creERT2 mice. *Plp1*-creERT2 mice were generated by Dr. Ueli Suter using a patented Cre-
677 ERT2 construct developed by Dr. Pierre Chambon at GIE-CERBM.
678

679 **COMPETING INTERESTS**

680 The authors declare no competing interests.
681

682 **FUNDINGS**

683 This work was supported by grants from Shriners Children's (#84050 to Y-J.S.) and NIH NINDS
684 (NS105796 to Y-J.S.).
685

686 **REFERENCES**

687

688 Beirowski, B., Babetto, E., Golden, J. P., Chen, Y. J., Yang, K., Gross, R. W., . . . Milbrandt, J.
689 (2014). Metabolic regulator LKB1 is crucial for Schwann cell-mediated axon maintenance.
690 *Nat Neurosci, 17*(10), 1351-1361. doi:10.1038/nn.3809
691 Beverdam, A., Claxton, C., Zhang, X., James, G., Harvey, K. F., & Key, B. (2013). Yap controls
692 stem/progenitor cell proliferation in the mouse postnatal epidermis. *J Invest Dermatol,*
693 *133*(6), 1497-1505. doi:10.1038/jid.2012.430
694 Bremer, M., Frob, F., Kichko, T., Reeh, P., Tamm, E. R., Suter, U., & Wegner, M. (2011). Sox10
695 is required for Schwann-cell homeostasis and myelin maintenance in the adult peripheral
696 nerve. *Glia, 59*(7), 1022-1032. doi:10.1002/glia.21173
697 Clemence, A., Mirsky, R., & Jessen, K. R. (1989). Non-myelin-forming Schwann cells proliferate
698 rapidly during Wallerian degeneration in the rat sciatic nerve. *J Neurocytol, 18*(2), 185-
699 192.
700 Decker, L., Desmarquet-Trin-Dinh, C., Taillebourg, E., Ghislain, J., Vallat, J. M., & Charnay, P.
701 (2006). Peripheral myelin maintenance is a dynamic process requiring constant Krox20
702 expression. *J Neurosci, 26*(38), 9771-9779. doi:10.1523/JNEUROSCI.0716-06.2006

Deng, Y., Wu, L. M. N., Bai, S., Zhao, C., Wang, H., Wang, J., . . . Lu, Q. R. (2017). A reciprocal regulatory loop between TAZ/YAP and G-protein Galphas regulates Schwann cell proliferation and myelination. *Nat Commun, 8*, 15161. doi:10.1038/ncomms15161

Diepenbruck, M., Waldmeier, L., Ivanek, R., Berninger, P., Arnold, P., van Nimwegen, E., & Christofori, G. (2014). Tead2 expression levels control the subcellular distribution of Yap and Taz, zyxin expression and epithelial-mesenchymal transition. *J Cell Sci, 127*(Pt 7), 1523-1536. doi:10.1242/jcs.139865

Feltri, M. L., D'Antonio, M., Previtali, S., Fasolini, M., Messing, A., & Wrabetz, L. (1999). P0-Cre transgenic mice for inactivation of adhesion molecules in Schwann cells. *Ann N Y Acad Sci, 883*, 116-123.

Feltri, M. L., Poitelon, Y., & Previtali, S. C. (2016). How Schwann Cells Sort Axons: New Concepts. *Neuroscientist, 22*(3), 252-265. doi:10.1177/1073858415572361

Fernando, R. N., Cotter, L., Perrin-Tricaud, C., Berthelot, J., Bartolami, S., Pereira, J. A., . . . Tricaud, N. (2016). Optimal myelin elongation relies on YAP activation by axonal growth and inhibition by Crb3/Hippo pathway. *Nat Commun, 7*, 12186. doi:10.1038/ncomms12186

Finzsch, M., Schreiner, S., Kichko, T., Reeh, P., Tamm, E. R., Bosl, M. R., . . . Wegner, M. (2010). Sox10 is required for Schwann cell identity and progression beyond the immature Schwann cell stage. *J Cell Biol, 189*(4), 701-712. doi:10.1083/jcb.200912142

Gerber, D., Pereira, J. A., Gerber, J., Tan, G., Dimitrieva, S., Yángüez, E., & Suter, U. (2021). Transcriptional profiling of mouse peripheral nerves to the single-cell level to build a sciatic nerve ATlas (SNAT). *Elife, 10*. doi:10.7554/eLife.58591

Ghislain, J., & Charnay, P. (2006). Control of myelination in Schwann cells: a Krox20 cis-regulatory element integrates Oct6, Brn2 and Sox10 activities. *EMBO Rep, 7*(1), 52-58. doi:10.1038/sj.embor.7400573

Gomez-Sanchez, J. A., Lopez de Armentia, M., Lujan, R., Kessaris, N., Richardson, W. D., & Cabedo, H. (2009). Sustained axon-glial signaling induces Schwann cell hyperproliferation, Remak bundle myelination, and tumorigenesis. *J Neurosci, 29*(36), 11304-11315. doi:10.1523/jneurosci.1753-09.2009

Grove, M., Kim, H., Santerre, M., Krupka, A. J., Han, S. B., Zhai, J., . . . Son, Y. J. (2017). YAP/TAZ initiate and maintain Schwann cell myelination. *Elife, 6*. doi:10.7554/eLife.20982

Grove, M., Lee, H., Zhao, H., & Son, Y. J. (2020). Axon-dependent expression of YAP/TAZ mediates Schwann cell remyelination but not proliferation after nerve injury. *Elife, 9*. doi:10.7554/eLife.50138

Hao, Y., Chun, A., Cheung, K., Rashidi, B., & Yang, X. (2008). Tumor Suppressor LATS1 Is a Negative Regulator of Oncogene YAP*. *Journal of Biological Chemistry, 283*(9), 5496-5509. doi:https://doi.org/10.1074/jbc.M709037200

Harty, B. L., & Monk, K. R. (2017). Unwrapping the unappreciated: recent progress in Remak Schwann cell biology. *Curr Opin Neurobiol, 47*, 131-137. doi:10.1016/j.conb.2017.10.003

He, X., Zhang, L., Queme, L. F., Liu, X., Lu, A., Waclaw, R. R., . . . Lu, Q. R. (2018). A histone deacetylase 3-dependent pathway delimits peripheral myelin growth and functional regeneration. *Nat Med, 24*(3), 338-351. doi:10.1038/nm.4483

He, Y., Kim, J. Y., Dupree, J., Tewari, A., Melendez-Vasquez, C., Svaren, J., & Casaccia, P. (2010). Yy1 as a molecular link between neuregulin and transcriptional modulation of peripheral myelination. *Nat Neurosci, 13*(12), 1472-1480. doi:10.1038/nn.2686

Heinz, S., Romanoski, C. E., Benner, C., & Glass, C. K. (2015). The selection and function of cell type-specific enhancers. *Nat Rev Mol Cell Biol, 16*(3), 144-154. doi:10.1038/nrm3949

Hindley, C., & Philpott, A. (2012). Co-ordination of cell cycle and differentiation in the developing nervous system. *Biochem J, 444*(3), 375-382. doi:10.1042/BJ20112040

Holden, J. K., & Cunningham, C. N. (2018). Targeting the Hippo Pathway and Cancer through the TEAD Family of Transcription Factors. *Cancers (Basel), 10*(3). doi:10.3390/cancers10030081

Hu, J. K., Du, W., Shelton, S. J., Oldham, M. C., DiPersio, C. M., & Klein, O. D. (2017). An FAK-YAP-mTOR Signaling Axis Regulates Stem Cell-Based Tissue Renewal in Mice. *Cell Stem Cell, 21*(1), 91-106 e106. doi:10.1016/j.stem.2017.03.023

Jaegle, M., Ghazvini, M., Mandemakers, W., Piirsoo, M., Driegen, S., Levavasseur, F., . . . Meijer, D. (2003). The POU proteins Brn-2 and Oct-6 share important functions in Schwann cell development. *Genes Dev, 17*(11), 1380-1391. doi:10.1101/gad.258203

Jang, S. W., Srinivasan, R., Jones, E. A., Sun, G., Keles, S., Krueger, C., . . . Svaren, J. (2010). Locus-wide identification of Egr2/Krox20 regulatory targets in myelin genes. *J Neurochem, 115*(6), 1409-1420. doi:10.1111/j.1471-4159.2010.07045.x

Jang, S. W., & Svaren, J. (2009). Induction of myelin protein zero by early growth response 2 through upstream and intragenic elements. *J Biol Chem, 284*(30), 20111-20120. doi:10.1074/jbc.M109.022426

Jeanette, H., Marziali, L. N., Bhatia, U., Hellman, A., Herron, J., Kopec, A. M., . . . Belin, S. (2021). YAP and TAZ regulate Schwann cell proliferation and differentiation during peripheral nerve regeneration. *Glia, 69*(4), 1061-1074. doi:10.1002/glia.23949

Jessen, K. R., & Mirsky, R. (2005). The origin and development of glial cells in peripheral nerves. *Nat Rev Neurosci, 6*(9), 671-682.

Jessen, K. R., & Mirsky, R. (2016). The repair Schwann cell and its function in regenerating nerves. *J Physiol, 594*(13), 3521-3531. doi:10.1113/jp270874

Jones, E. A., Jang, S. W., Mager, G. M., Chang, L. W., Srinivasan, R., Gokey, N. G., . . . Svaren, J. (2007). Interactions of Sox10 and Egr2 in myelin gene regulation. *Neuron Glia Biol, 3*(4), 377-387. doi:10.1017/S1740925X08000173

Kao, S. C., Wu, H., Xie, J., Chang, C. P., Ranish, J. A., Graef, I. A., & Crabtree, G. R. (2009). Calcineurin/NFAT signaling is required for neuregulin-regulated Schwann cell differentiation. *Science, 323*(5914), 651-654.

Kim, J., Kwon, H., Shin, Y. K., Song, G., Lee, T., Kim, Y., . . . Jho, E. H. (2020). MAML1/2 promote YAP/TAZ nuclear localization and tumorigenesis. *Proc Natl Acad Sci U S A, 117*(24), 13529-13540. doi:10.1073/pnas.1917969117

Kim, M., Kim, T., Johnson, R. L., & Lim, D. S. (2015). Transcriptional co-repressor function of the hippo pathway transducers YAP and TAZ. *Cell Rep, 11*(2), 270-282. doi:10.1016/j.celrep.2015.03.015

Kim, M., Wende, H., Walcher, J., Kuhnemund, J., Cheret, C., Kempa, S., . . . Birchmeier, C. (2018). Maf links Neuregulin1 signaling to cholesterol synthesis in myelinating Schwann cells. *Genes Dev, 32*(9-10), 645-657. doi:10.1101/gad.310490.117

Kofler, M., Speight, P., Little, D., Di Ciano-Oliveira, C., Szaszi, K., & Kapus, A. (2018). Mediated nuclear import and export of TAZ and the underlying molecular requirements. *Nat Commun, 9*(1), 4966. doi:10.1038/s41467-018-07450-0

Le, N., Nagarajan, R., Wang, J. Y., Araki, T., Schmidt, R. E., & Milbrandt, J. (2005). Analysis of congenital hypomyelinating Egr2Lo/Lo nerves identifies Sox2 as an inhibitor of Schwann

795 cell differentiation and myelination. *Proc Natl Acad Sci U S A, 102*(7), 2596-2601.
796 doi:10.1073/pnas.0407836102
797 Le, N., Nagarajan, R., Wang, J. Y., Svaren, J., LaPash, C., Araki, T., . . . Milbrandt, J. (2005). Nab
798 proteins are essential for peripheral nervous system myelination. *Nat Neurosci, 8*(7), 932-
799 940. doi:10.1038/nn1490
800 LeBlanc, S. E., Jang, S. W., Ward, R. M., Wrabetz, L., & Svaren, J. (2006). Direct regulation of
801 myelin protein zero expression by the Egr2 transactivator. *J Biol Chem, 281*(9), 5453-5460.
802 doi:10.1074/jbc.M512159200
803 Leblanc, S. E., Srinivasan, R., Ferri, C., Mager, G. M., Gillian-Daniel, A. L., Wrabetz, L., &
804 Svaren, J. (2005). Regulation of cholesterol/lipid biosynthetic genes by Egr2/Krox20
805 during peripheral nerve myelination. *J Neurochem, 93*(3), 737-748. doi:10.1111/j.1471-
806 4159.2005.03056.x
807 Leone, D. P., Genoud, S., Atanasoski, S., Grausenburger, R., Berger, P., Metzger, D., . . . Suter,
808 U. (2003). Tamoxifen-inducible glia-specific Cre mice for somatic mutagenesis in
809 oligodendrocytes and Schwann cells. *Mol Cell Neurosci, 22*(4), 430-440.
810 Li, Z., Zhao, B., Wang, P., Chen, F., Dong, Z., Yang, H., . . . Xu, Y. (2010). Structural insights
811 into the YAP and TEAD complex. *Genes Dev, 24*(3), 235-240. doi:10.1101/gad.1865810
812 Liu, R., Jagannathan, R., Li, F., Lee, J., Balasubramanyam, N., Kim, B. S., . . . Moulik, M. (2019).
813 Tead1 is required for perinatal cardiomyocyte proliferation. *PLoS One, 14*(2), e0212017.
814 doi:10.1371/journal.pone.0212017
815 Lopez-Anido, C., Poitelon, Y., Gopinath, C., Moran, J. J., Ma, K. H., Law, W. D., . . . Svaren, J.
816 (2016). Tead1 regulates the expression of Peripheral Myelin Protein 22 during Schwann
817 cell development. *Hum Mol Genet*. doi:10.1093/hmg/ddw158
818 Lopez-Anido, C., Sun, G., Koenning, M., Srinivasan, R., Hung, H. A., Emery, B., . . . Svaren, J.
819 (2015). Differential Sox10 genomic occupancy in myelinating glia. *Glia*.
820 doi:10.1002/glia.22855
821 Montani, L., Pereira, J. A., Norrmen, C., Pohl, H. B. F., Tinelli, E., Trotzmuller, M., . . . Suter, U.
822 (2018). De novo fatty acid synthesis by Schwann cells is essential for peripheral nervous
823 system myelination. *J Cell Biol, 217*(4), 1353-1368. doi:10.1083/jcb.201706010
824 Monuki, E. S., Kuhn, R., & Lemke, G. (1993). Repression of the myelin P0 gene by the POU
825 transcription factor SCIP. *Mech Dev, 42*(1-2), 15-32. doi:10.1016/0925-4773(93)90095-f
826 Mukhtar, T., Breda, J., Grison, A., Karimaddini, Z., Grobecker, P., Iber, D., . . . Taylor, V. (2020).
827 Tead transcription factors differentially regulate cortical development. *Sci Rep, 10*(1), 4625.
828 doi:10.1038/s41598-020-61490-5
829 Norrmen, C., Figlia, G., Lebrun-Julien, F., Pereira, J. A., Trotzmuller, M., Kofeler, H. C., . . . Suter,
830 U. (2014). mTORC1 controls PNS myelination along the mTORC1-RXRgamma-SREBP-
831 lipid biosynthesis axis in Schwann cells. *Cell Rep, 9*(2), 646-660.
832 doi:10.1016/j.celrep.2014.09.001
833 Norrmén, C., Figlia, G., Pfistner, P., Pereira, J. A., Bachofner, S., & Suter, U. (2018). mTORC1
834 Is Transiently Reactivated in Injured Nerves to Promote c-Jun Elevation and Schwann Cell
835 Dedifferentiation. *J Neurosci, 38*(20), 4811-4828. doi:10.1523/jneurosci.3619-17.2018
836 Poitelon, Y., Lopez-Anido, C., Catignas, K., Berti, C., Palmisano, M., Williamson, C., . . . Feltri,
837 M. L. (2016). YAP and TAZ control peripheral myelination and the expression of laminin
838 receptors in Schwann cells. *Nat Neurosci, 19*(7), 879-887. doi:10.1038/nn.4316
839 Rasi, K., Hurskainen, M., Kallio, M., Staven, S., Sormunen, R., Heape, A. M., . . . Pihlajaniemi,
840 T. (2010). Lack of collagen XV impairs peripheral nerve maturation and, when combined

with laminin-411 deficiency, leads to basement membrane abnormalities and sensorimotor dysfunction. *J Neurosci, 30*(43), 14490-14501. doi:10.1523/JNEUROSCI.2644-10.2010

Ren, B., & Yue, F. (2015). Transcriptional Enhancers: Bridging the Genome and Phenome. *Cold Spring Harb Symp Quant Biol, 80*, 17-26. doi:10.1101/sqb.2015.80.027219

Ryu, E. J., Wang, J. Y., Le, N., Baloh, R. H., Gustin, J. A., Schmidt, R. E., & Milbrandt, J. (2007). Misexpression of Pou3f1 results in peripheral nerve hypomyelination and axonal loss. *J Neurosci, 27*(43), 11552-11559. doi:10.1523/JNEUROSCI.5497-06.2007

Saher, G., Quintes, S., Mobius, W., Wehr, M. C., Kramer-Albers, E. M., Brugger, B., & Nave, K. A. (2009). Cholesterol regulates the endoplasmic reticulum exit of the major membrane protein P0 required for peripheral myelin compaction. *J Neurosci, 29*(19), 6094-6104. doi:10.1523/JNEUROSCI.0686-09.2009

Salzer, J. L. (2015). Schwann cell myelination. *Cold Spring Harb Perspect Biol, 7*(8), a020529. doi:10.1101/cshperspect.a020529

Scherer, S. S., & Wrabetz, L. (2008). Molecular mechanisms of inherited demyelinating neuropathies. *Glia, 56*(14), 1578-1589. doi:10.1002/glia.20751

Schulz, A., Walther, C., Morrison, H., & Bauer, R. (2014). In vivo electrophysiological measurements on mouse sciatic nerves. *J Vis Exp*(86). doi:10.3791/51181

Sherman, D. L., Krols, M., Wu, L. M., Grove, M., Nave, K. A., Gangloff, Y. G., & Brophy, P. J. (2012). Arrest of myelination and reduced axon growth when Schwann cells lack mTOR. *J Neurosci, 32*(5), 1817-1825. doi:10.1523/JNEUROSCI.4814-11.2012

Son, Y. J., & Thompson, W. J. (1995). Schwann cell processes guide regeneration of peripheral axons. *Neuron, 14*(1), 125-132. doi:0896-6273(95)90246-5 [pii]

Taveggia, C., Zanazzi, G., Petrylak, A., Yano, H., Rosenbluth, J., Einheber, S., . . . Salzer, J. L. (2005). Neuregulin-1 type III determines the ensheathment fate of axons. *Neuron, 47*(5), 681-694. doi:10.1016/j.neuron.2005.08.017

Tian, W., Yu, J., Tomchick, D. R., Pan, D., & Luo, X. (2010). Structural and functional analysis of the YAP-binding domain of human TEAD2. *Proc Natl Acad Sci U S A, 107*(16), 7293-7298. doi:10.1073/pnas.1000293107

Topilko, P., Schneider-Maunoury, S., Levi, G., Baron-Van Evercooren, A., Chennoufi, A. B., Seitanidou, T., . . . Charnay, P. (1994). Krox-20 controls myelination in the peripheral nervous system. *Nature, 371*(6500), 796-799. doi:10.1038/371796a0

Tricaud, N., & Park, H. T. (2017). Wallerian demyelination: chronicle of a cellular cataclysm. *Cell Mol Life Sci, 74*(22), 4049-4057. doi:10.1007/s00018-017-2565-2

Verheijen, M. H., Camargo, N., Verdier, V., Nadra, K., de Preux Charles, A. S., Medard, J. J., . . . Smit, A. B. (2009). SCAP is required for timely and proper myelin membrane synthesis. *Proc Natl Acad Sci U S A, 106*(50), 21383-21388. doi:10.1073/pnas.0905633106

Wen, T., Liu, J., He, X., Dong, K., Hu, G., Yu, L., . . . Zhou, J. (2019). Transcription factor TEAD1 is essential for vascular development by promoting vascular smooth muscle differentiation. *Cell Death Differ, 26*(12), 2790-2806. doi:10.1038/s41418-019-0335-4

Wen, T., Yin, Q., Yu, L., Hu, G., Liu, J., Zhang, W., . . . Zhou, J. (2017). Characterization of mice carrying a conditional TEAD1 allele. *Genesis, 55*(12). doi:10.1002/dvg.23085

Wright, M. C., Cho, W. J., & Son, Y. J. (2007). Distinct patterns of motor nerve terminal sprouting induced by ciliary neurotrophic factor vs. botulinum toxin. *J Comp Neurol, 504*(1), 1-16. doi:10.1002/cne.21439

Wu, S., Liu, Y., Zheng, Y., Dong, J., & Pan, D. (2008). The TEAD/TEF family protein Scalloped mediates transcriptional output of the Hippo growth-regulatory pathway. *Dev Cell, 14*(3), 388-398. doi:10.1016/j.devcel.2008.01.007

Yao, F., Zhou, Z., Kim, J., Hang, Q., Xiao, Z., Ton, B. N., . . . Ma, L. (2018). SKP2- and OTUD1-regulated non-proteolytic ubiquitination of YAP promotes YAP nuclear localization and activity. *Nat Commun, 9*(1), 2269. doi:10.1038/s41467-018-04620-y

Zhao, B., Wei, X., Li, W., Udan, R. S., Yang, Q., Kim, J., . . . Guan, K. L. (2007). Inactivation of YAP oncoprotein by the Hippo pathway is involved in cell contact inhibition and tissue growth control. *Genes Dev, 21*(21), 2747-2761. doi:10.1101/gad.1602907

Zhao, B., Ye, X., Yu, J., Li, L., Li, W., Li, S., . . . Guan, K. L. (2008). TEAD mediates YAP-dependent gene induction and growth control. *Genes Dev, 22*(14), 1962-1971. doi:10.1101/gad.1664408

Zheng, Y., & Pan, D. (2019). The Hippo Signaling Pathway in Development and Disease. *Dev Cell, 50*(3), 264-282. doi:10.1016/j.devcel.2019.06.003

Zorick, T. S., Syroid, D. E., Brown, A., Gridley, T., & Lemke, G. (1999). Krox-20 controls SCIP expression, cell cycle exit and susceptibility to apoptosis in developing myelinating Schwann cells. *Development, 126*(7), 1397-1406.

FIGURE LEGENDS

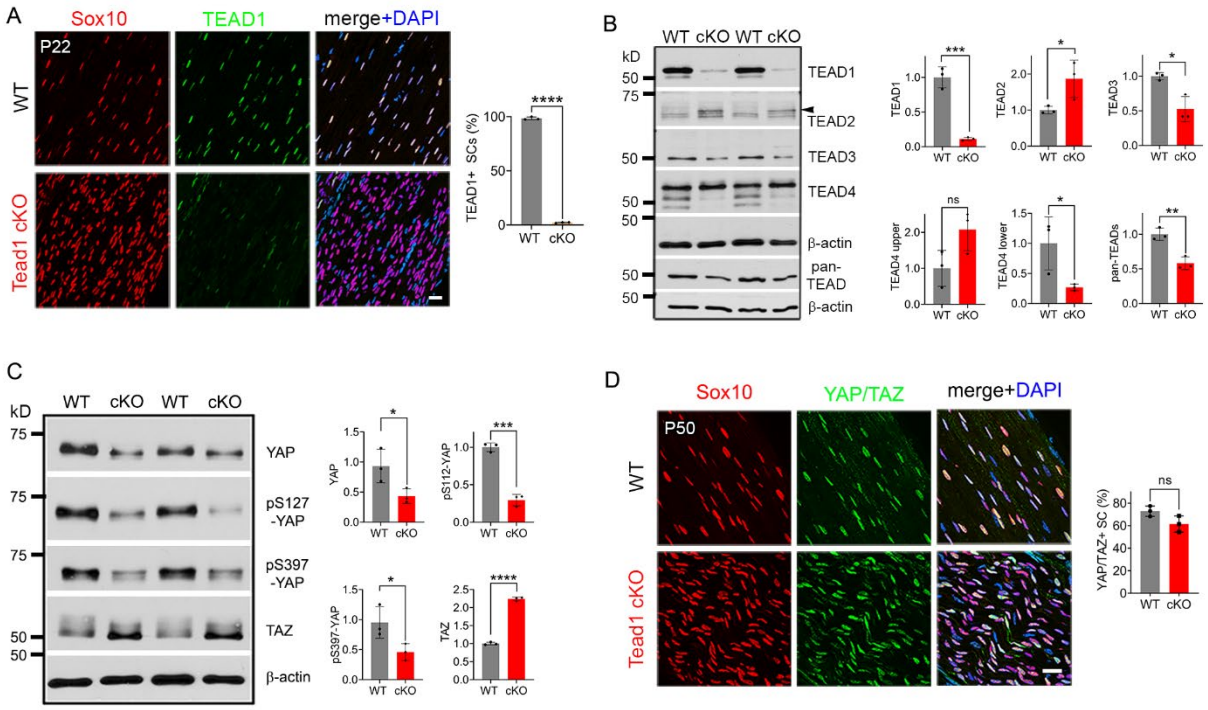

906

907 **Figure 1. Multiple TEADs are expressed in Schwann cells of WT and *Tead1* cKO mice**

908 **(A)** Immunostaining and quantification of TEAD1+ SCs on longitudinal sections of P22 WT and

909 *Tead1* cKO SNs. SC nuclei are identified by Sox10. All cell nuclei are marked by DAPI. n = 3

910 mice per genotype, ****P < 0.0001, Student's unpaired t-test. Scale bar: 20μm

911 **(B)** Western blotting of P50 WT and *Tead1* cKO SN lysates with anti-TEAD1, -TEAD2, -

912 TEAD3, -TEAD4, and -pan TEAD. TEAD expression is normalized to that of *β-actin* as an

913 internal control, and WT expression is arbitrarily given the value 1. n = 3 mice per genotype. ns,

914 p > 0.05; *p ≤ 0.05, **p ≤ 0.005, ***p ≤ 0.001, Student's unpaired t-test.

915

916 **(C)** Western blotting of P50 WT and *Tead1* cKO SN lysates with anti-YAP, -phospho-YAPs

917 (Ser127 and Ser397), and -TAZ. YAP/TAZ expression is normalized to that of *β-actin* as an

918 internal control, and WT expression is arbitrarily given the value 1. n = 3 mice per genotype. *p

919 ≤ 0.05, ***p ≤ 0.001, ****P < 0.0001, Student's unpaired t-test.

920 **(D)** Immunostaining of YAP/TAZ+ SCs on longitudinal sections of P50 WT and *Tead1* cKO

921 SNs. SC nuclei are identified by Sox10. All cell nuclei are marked by DAPI. n = 3 mice per

922 genotype, ns, p > 0.05, Student's unpaired t-test. Scale bar: 20μm

923

924 The following figure supplements are available for Figure 1.

925

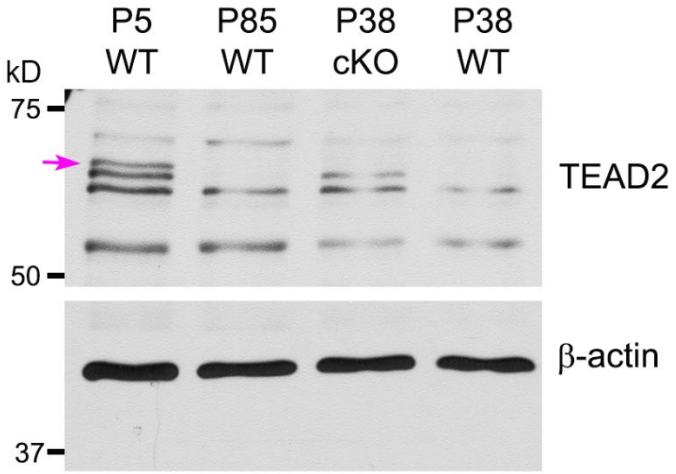

926

927

928 **Figure 1-figure supplement 1**

929 **Western blotting of P5, P38, P85 WT and P38 *Tead1* cKO SN lysates with anti-TEAD2**

930 TEAD2 expression is normalized to that of *β-actin* as an internal control. Arrow denotes ~65 kD
931 TEAD2 band that was diminished with age.

932

933 **Source data 1**

934 This zip archive contains source files for graphs in figure 1A, 1B, 1C, 1D and uncropped labeled
935 or unlabeled blots of figure 1B and 1D.

936

937 **Source data 2**

938 This zip archive contains uncropped labeled or unlabeled blots in **Figure 1-figure supplement 1.**

939

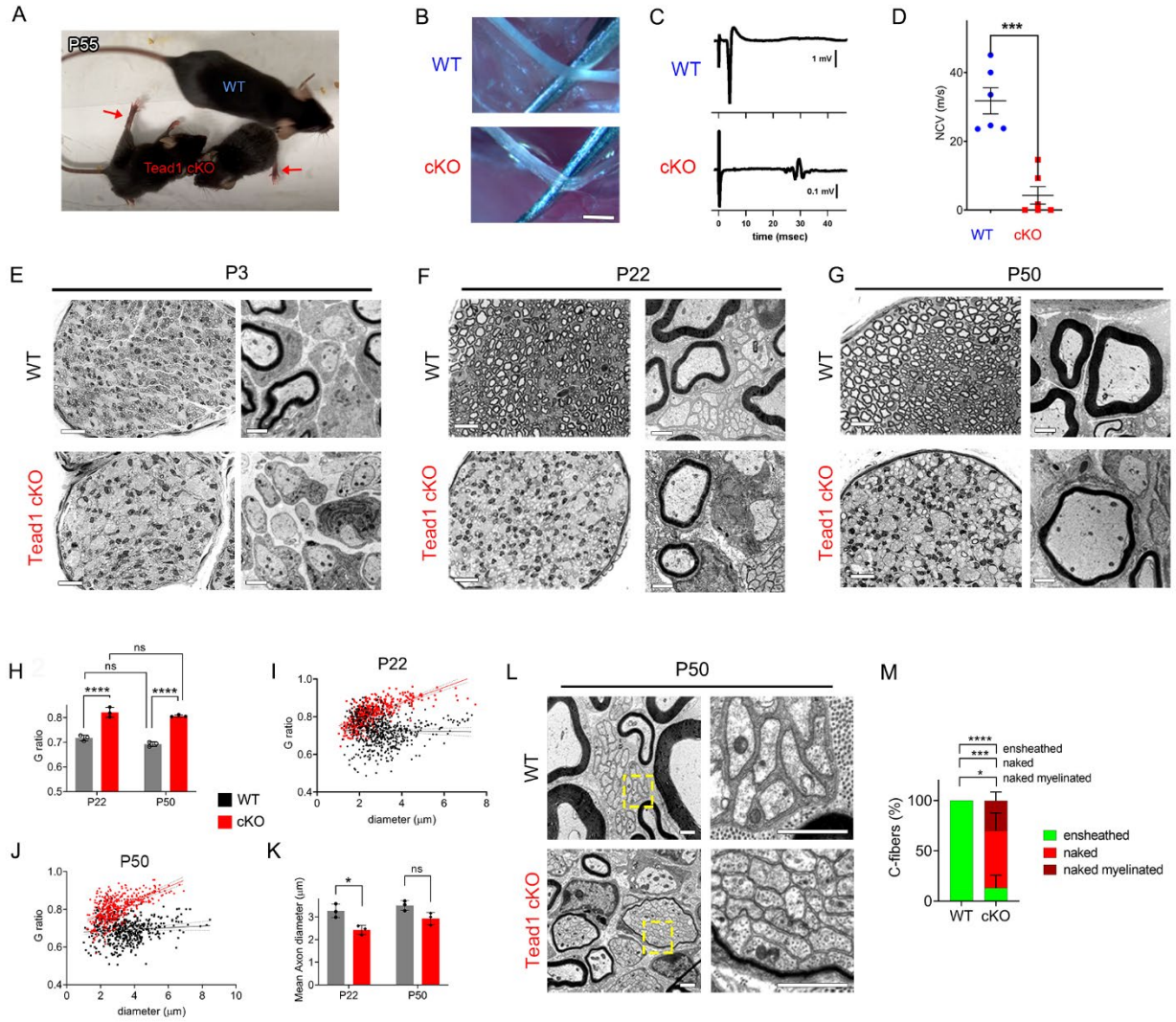

Figure 2. TEAD1 is required for myelin sheath formation and growth

(A) A living control (WT) and two *Tead1* cKO mice from one litter at P55. Arrows point to splayed paralyzed hindlimbs.

(B) Exposed SNs of WT and *Tead1* cKO mice during dissection. Scale bar: 1mm

(C) Representative images of CMAPs generated by stimulation of WT and *Tead1* cKO SNs.

(D) Quantification of NCV in WT and *Tead1* cKO. n = 6 mice per genotype. ***P < 0.001, Student's unpaired t-test.

(E) Representative images of semithin (left panels) and TEM (right panels) of transverse sections of WT and *Tead1* cKO SNs at P3. Scale bar: 20µm (left panels), 1µm (right panels)

951 **(F)** Representative images of semithin (left panels) and TEM (right panels) of transverse sections
952 of WT and *Tead1* cKO SNs at P22. Scale bar: 20μm (left panels), 1μm (right panels)
953 **(G)** Representative images of semithin (left panels) and TEM (right panels) of transverse
954 sections of WT and *Tead1* cKO SNs at P50. Scale bar: 20μm (left panels), 1μm (right panels)
955 **(H)** Quantification of G-ratio for axons in WT and *Tead1* cKO SNs at P22 and at P50. n = 3
956 mice per group. ns, $p > 0.05$ (P22 WT versus P50 WT, P22 cKO versus P50 cKO), ****$P <$
957 0.0001 (P22 WT versus P22 cKO, P50 WT versus P50 cKO).
958 **(I)** Scatter plot graph displaying G-ratio in relation to axon diameter in WT and *Tead1* cKO SNs
959 at P22. n = 1063 axons from 3 mice per each genotype.
960 **(J)** Scatter plot graph displaying G-ratio in relation to axon diameter in WT and *Tead1* cKO SNs
961 at P50. n = 880 axons from 3 mice per each genotype.
962 **(K)** Quantitative comparison of mean axon diameter in WT and *Tead1* cKO SNs at P22 and at
963 P50. n = 3 mice per group. ns, $p > 0.05$, *$p \leq 0.05$, 2-way ANOVA with Tukey's multiple
964 comparisons test.
965 **(L)** Representative TEM images of transverse sections of P50 WT and *Tead1* cKO SNs. Right
966 panels are enlarged images of the boxed area in left panels. Scale bar: 1μm
967 **(M)** Quantification of normal and abnormal C-fibers in P50 WT and *Tead1* cKO SNs. C-fibers
968 normally ensheathed by SC cytoplasm are marked as 'ensheathed', whereas those not ensheathed
969 are denoted as 'naked'. Naked C-fibers located in a myelinated bundle are denoted as 'naked
970 myelinated'. Relative percentage of each type of C-fiber is plotted. N > 500 C-fibers from 3 mice
971 per each genotype. *$p \leq 0.05$, ***$p \leq 0.001$, ****$P < 0.0001$, 2-way ANOVA Tukey's multiple
972 comparisons test.
973
974 The following figure supplements are available for Figure 2.

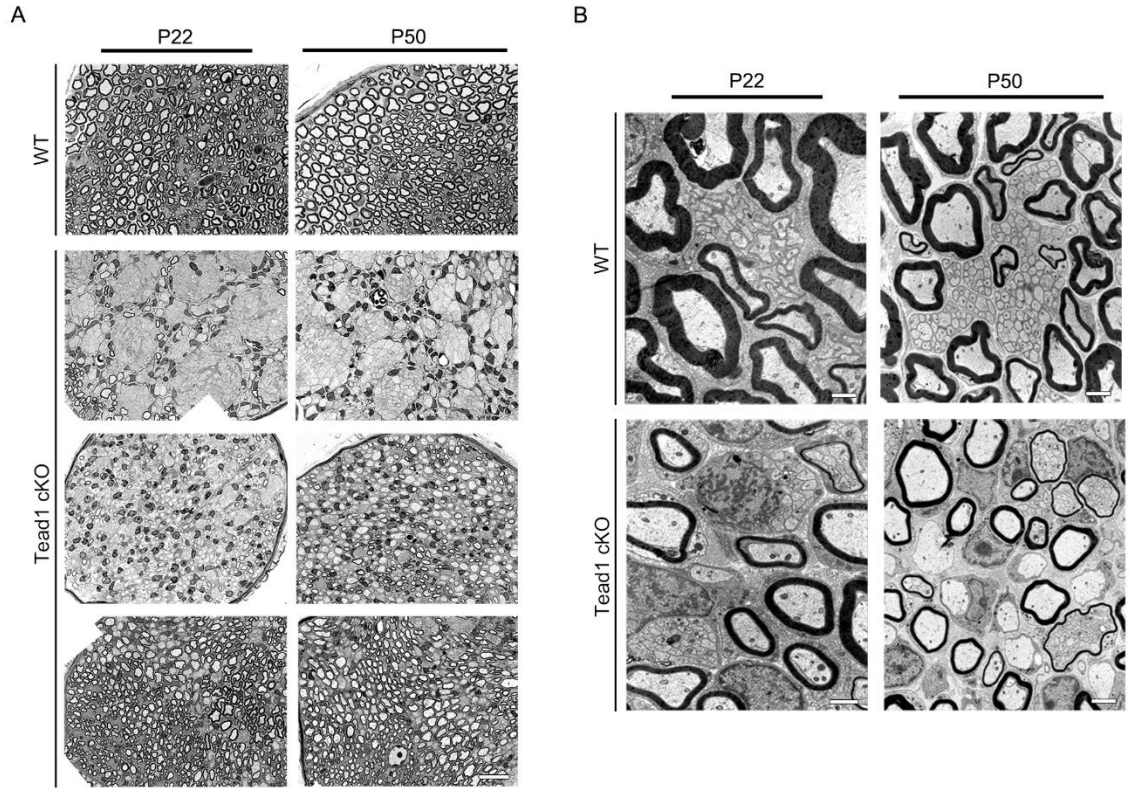

975

976 **Figure 2-figure supplement 1**

977 **Additional semi-thin and TEM images of WT and *Tead1* cKO**

978 **(A)** Representative images of semi-thin sections of various areas of WT and Tead1 cKO SNs at

979 P22 and P50. Scale bar: 20μm

980 **(B)** Representative TEM images of transverse sections of WT and Tead1 cKO SNs at P22 and

981 P50. Scale bar: 1μm (P22 panels), 2μm (P50 panels)

982

983 **Source data 1**

984 This zip archive contains source files for graphs in Figure 2D, 2H, 2I, 2J, 2K, 2M.

985

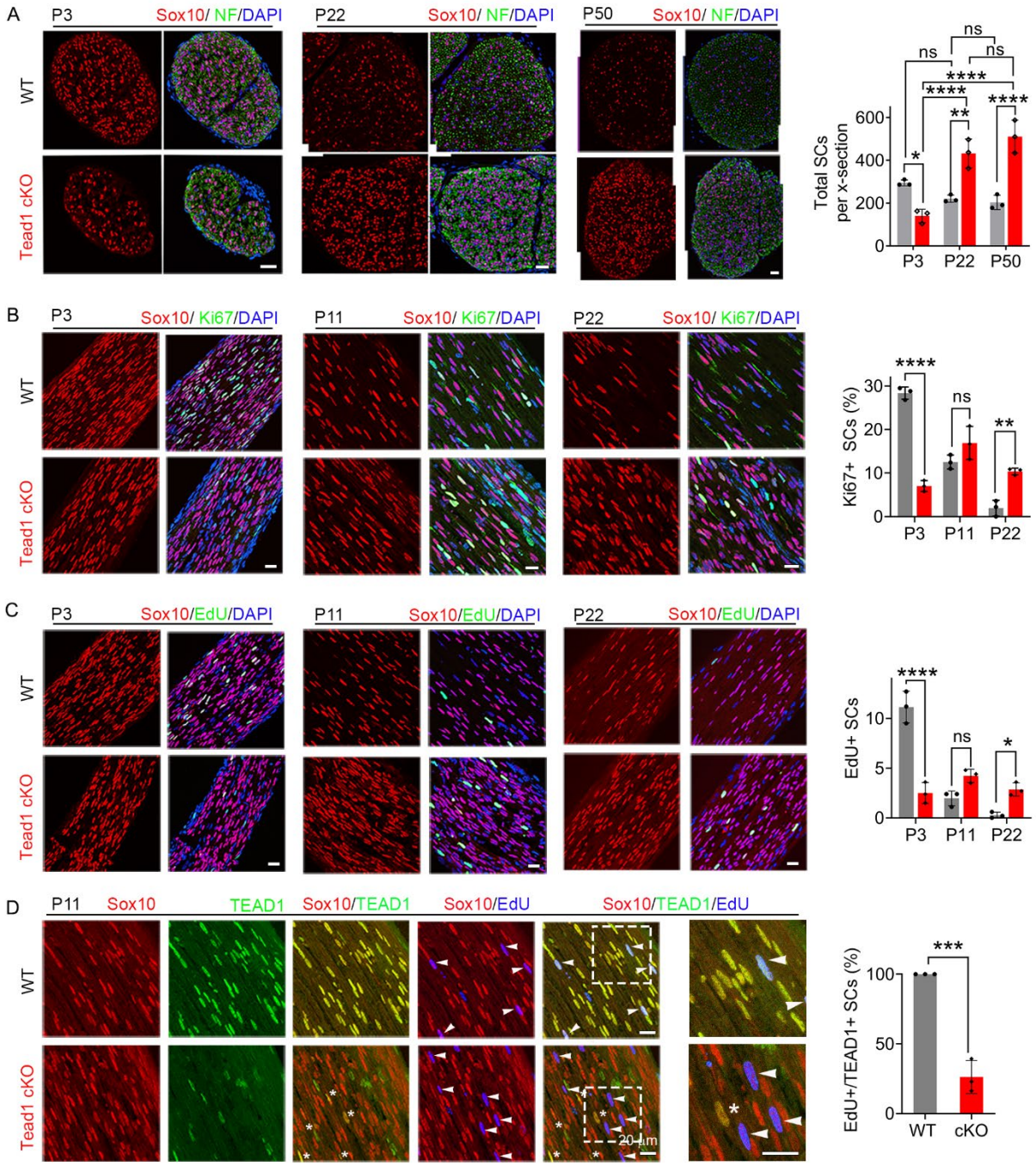

Figure 3. TEAD1 regulates SC proliferation both positively and negatively

(A) Immunostaining and quantification of SCs on transverse sections of WT and *Tead1* cKO SNs at P3, P22, and P52. SC nuclei and all cell nuclei are marked by Sox10 and DAPI. Axons

991 are marked by Neurofilaments (NF). n = 3 mice per genotype, ns, $p > 0.05$, *$p \leq 0.05$, **$p \leq$
992 0.01, ****$P < 0.0001$, 2-way ANOVA with Tukey's multiple comparisons test. Scale bar: 30µm
993 **(B)** Immunostaining and quantification of Ki67+ SCs on longitudinal sections of WT and *Tead1*
994 cKO SNs at P3, P11, and P22. SC nuclei and all cell nuclei are marked by Sox10 and DAPI. n =
995 3 mice per genotype, ns, $p > 0.05$, **$p \leq 0.01$, ****$P < 0.0001$, 2-way ANOVA with Tukey's
996 multiple comparisons test. Scale bar: 30µm (P3 panels), 20µm (P11 and P22 panels)
997 **(C)** Immunostaining and quantification of EdU+ SCs on longitudinal sections of WT and *Tead1*
998 cKO SNs at P3, P11, and P22. SC nuclei and all cell nuclei are marked by Sox10 and DAPI. n =
999 3 mice per genotype, ns, $p > 0.05$, *$p \leq 0.05$, ****$P < 0.0001$, 2-way ANOVA with Tukey's
1000 multiple comparisons test. Scale bar: 30µm (P3 panels), 20µm (P11 and P22 panels)
1001 **(D)** Immunostaining and quantification of EdU+/TEAD1+ SCs on longitudinal sections of WT
1002 and *Tead1* cKO SNs at P11. SC nuclei are marked by Sox10. Asterisks denote *Tead1* cKO SCs
1003 in which TEAD1 is not deleted and which are not EdU+. Arrowheads denote EdU+ SCs which
1004 are TEAD1+ in WT but TEAD1- in *Tead1* cKO. n = 3 mice per genotype, ***$P < 0.001$,
1005 Student's unpaired t-test. Scale bar: 20µm
1006
1007 The following figure supplements are available for Figure 3.
1008
1009 **Source data 1**
1010 This zip archive contains source files for graphs in Figure 3A, 3B, 3C, 3D.
1011

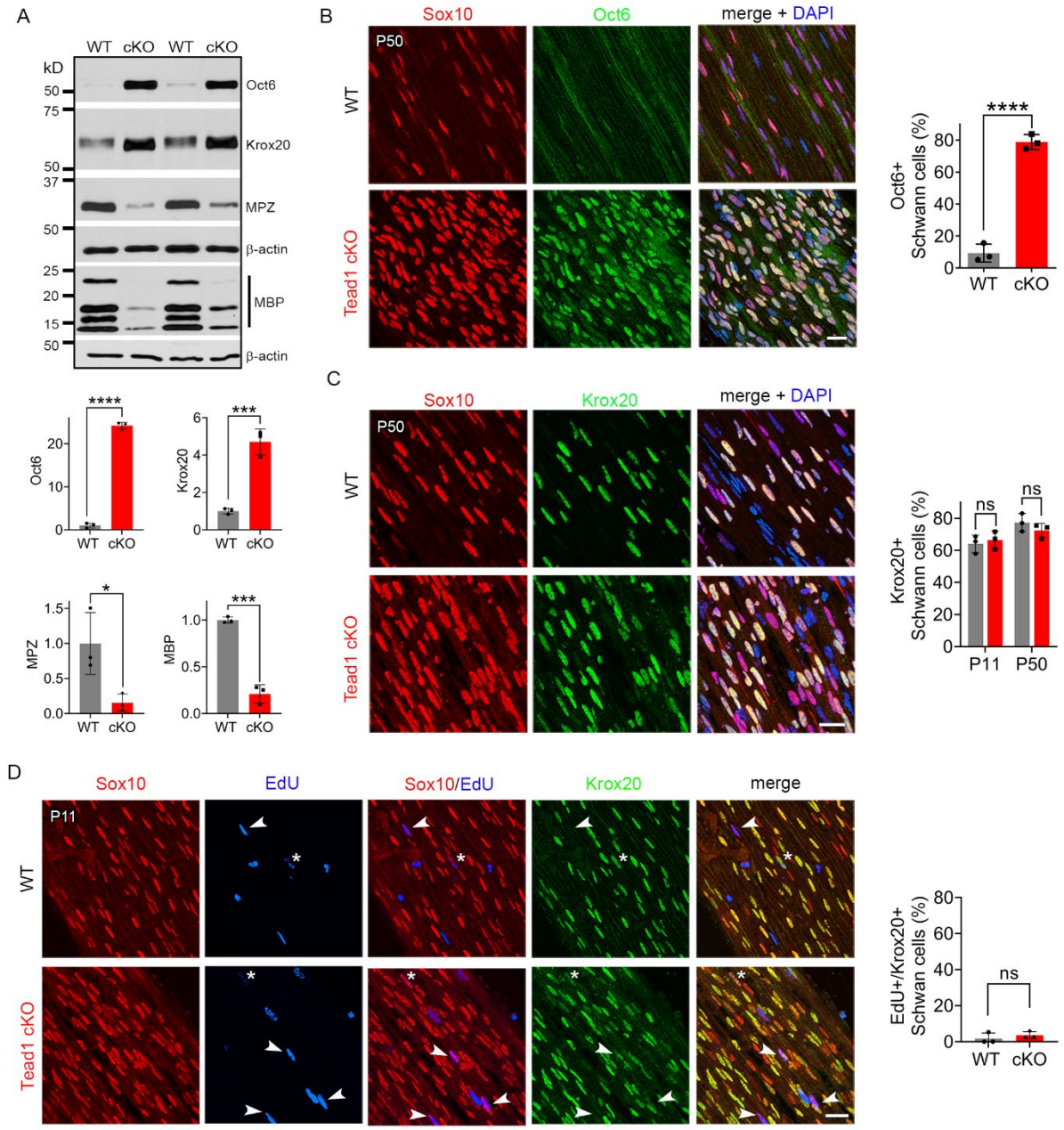

Figure 4. TEAD1 is required for Krox20 to upregulate myelin proteins during development

(A) Western blotting of P50 WT and *Tead1* cKO SN lysates with anti-Oct6, -Krox20, -MPZ, and -MBP. Protein expression is normalized to that of *β-actin* as an internal control, and WT expression is arbitrarily given the value 1. n = 3 mice per genotype. *p ≤ 0.05, ***p ≤ 0.001, ***p ≤ 0.0001, Student's unpaired t-test.

1020 **(B)** Immunostaining and quantification of Oct6+ SCs on longitudinal sections of P50 WT and
1021 *Tead1* cKO SNs. SC nuclei are identified by Sox10. All cell nuclei are marked by DAPI. n = 3
1022 mice per genotype, ****P < 0.0001, Student's unpaired t-test. Scale bar: 20μm
1023 **(C)** Immunostaining and quantification of Krox20+ SCs on longitudinal sections of WT and
1024 *Tead1* cKO SNs at P11 and P50. SC nuclei are identified by Sox10. All cell nuclei are marked by
1025 DAPI. n = 3 mice per each group, ns, p > 0.05, Student's unpaired t-test. Scale bar: 20μm
1026 **(D)** Immunostaining and quantification of EdU+/Krox20+ SCs on longitudinal sections of WT
1027 and *Tead1* cKO SNs at P11. SC nuclei are identified by Sox10. Arrowheads denote examples of
1028 EdU+ SCs which are Krox20-. Asterisks denote rarely observed EdU+ SCs which are Krox20+.
1029 n = 3 mice per genotype, ns, p > 0.05, Student's unpaired t-test. Scale bar: 20μm
1030
1031 The following figure supplements are available for Figure 4.
1032
1033 **Source data 1**
1034 This zip archive contains source files for graphs in Figure 4A, 4B, 4C, 4D and uncropped labeled
1035 or unlabeled blots of Figure 4A.
1036

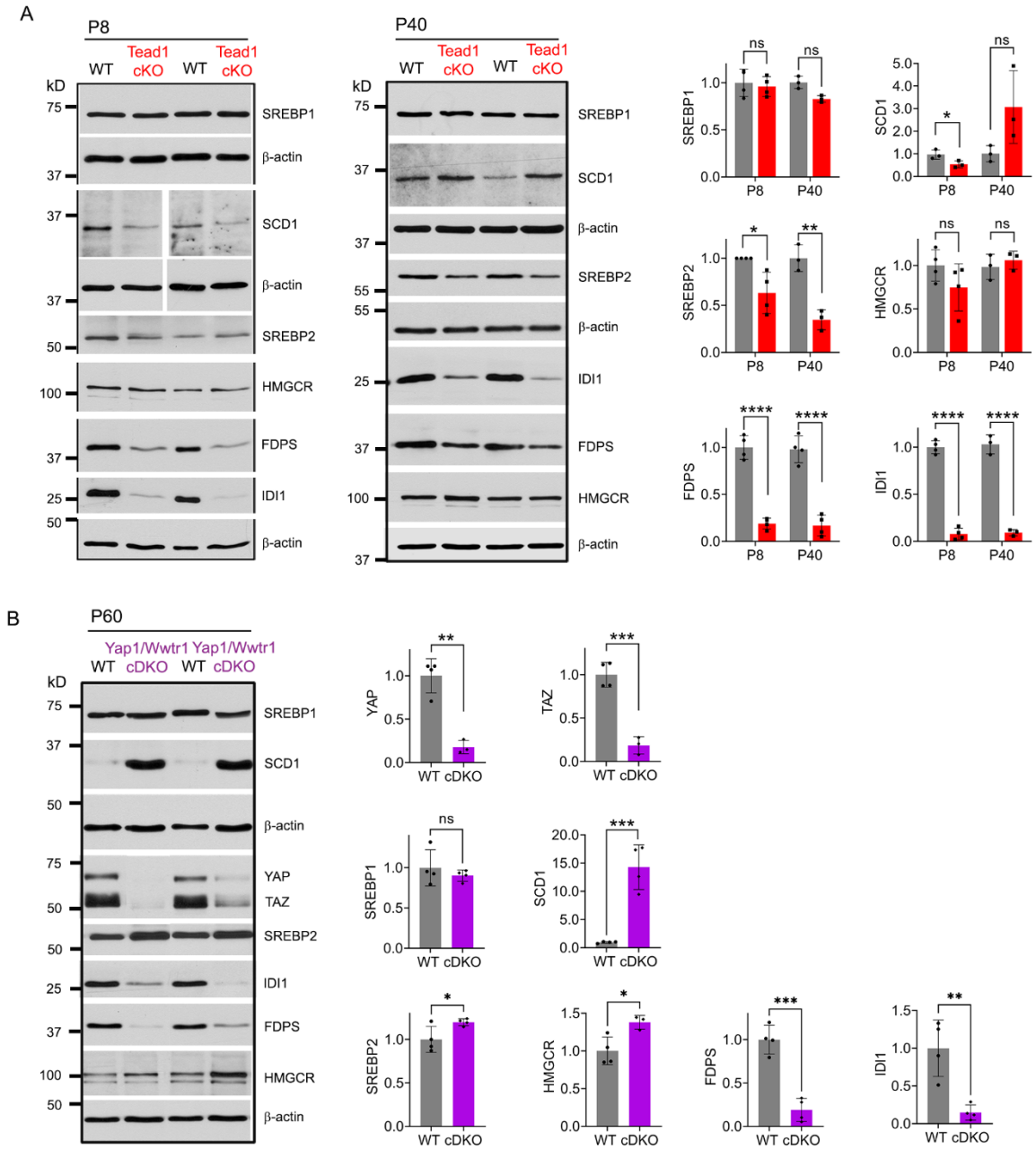

Figure 5. TEAD1 and YAP/TAZ upregulate cholesterol synthesis enzymes: FDPS and IDI1

(A) Western blotting of P8 and P40 WT and *Tead1* cKO SN lysates with anti-SREBP1, -SCD1, -SREBP2, -HMGCR, -FDPS, and -IDI1. Protein expression is normalized to that of *β-actin* as an internal control, and WT expression is arbitrarily given the value 1. n = 3 or 4 mice per genotype. ns, $p > 0.05$, *$p \leq 0.05$, **$p \leq 0.01$, ****$P < 0.0001$, Student's unpaired t-test.

1044 **(B)** Western blotting of P60 WT and *Yap1/Wwtr1* cDKO SN lysates with anti-YAP, -TAZ, -
1045 SREBP1, -SCD1, -SREBP2, -HMGCR, -FDPS, and -IDI1. Protein expression is normalized to
1046 that of *β-actin* as an internal control, and WT expression is arbitrarily given the value 1. n = 3 or
1047 4 mice per genotype. ns, $p > 0.05$, *$p \leq 0.05$, **$p \leq 0.01$, ***$P < 0.001$, Student's unpaired t-test.
1048
1049 The following figure supplements are available for Figure 5.
1050
1051 **Source data 1**
1052 This zip archive contains uncropped labeled or unlabeled blots of P8 WT and Tead1 cKO SNs in
1053 Figure 5A.
1054
1055 **Source data 2**
1056 This zip archive contains source files for graphs in Figure 5A and 5B, and uncropped labeled or
1057 unlabeled blots of P40 WT and Tead1 cKO SNs in Figure 5A, and P60 SNs of WT and
1058 YAP/TAZ cDKO in Figure 5B.
1059

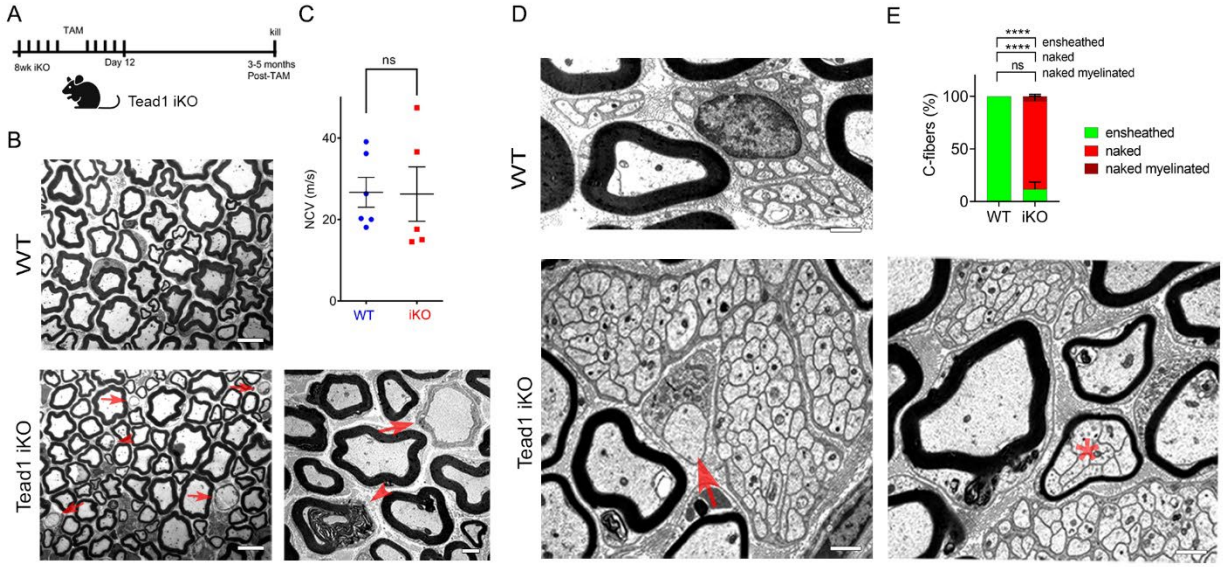

1060
1061
1062 **Figure 6. TEAD1 is largely dispensable for myelin maintenance, but required for Remak**
1063 **bundle integrity**
1064 **(A)** Cartoon showing timeline of tamoxifen (TAM) injection and time of sacrifice of *Tead1* iKO
1065 mice.

1066 **(B)** Representative TEM images of P150 WT and *Tead1* iKO SNs showing occasional large
1067 axons undergoing demyelination (arrowheads) or completely demyelinated (arrows). Scale bar:
1068 6μm (left panels), 2μm (right panel)
1069 **(C)** Quantification of NCV in P90-P150 WT and *Tead1* iKO mice. n = 5 or 6 mice per genotype.
1070 ns, $p > 0.05$, Student's unpaired t-test.
1071 **(D)** Representative TEM images of P97 WT and *Tead1* iKO SNs showing Remak bundles.
1072 Asterisk denotes a bundle of thinly myelinated C-fibers. Arrow denotes demyelinated axon.
1073 Scale bar: 1μm
1074 **(E)** Quantification of normal and abnormal C-fibers in P150 WT and *Tead1* iKO SNs. Relative
1075 percentage of each type of C-fiber is plotted. N > 500 C-fibers from 3 mice per each genotype.
1076 ns, $p > 0.05$, ****$P < 0.0001$, 2-way ANOVA with Tukey's multiple comparisons test.
1077
1078 The following figure supplements are available for Figure 6.
1079

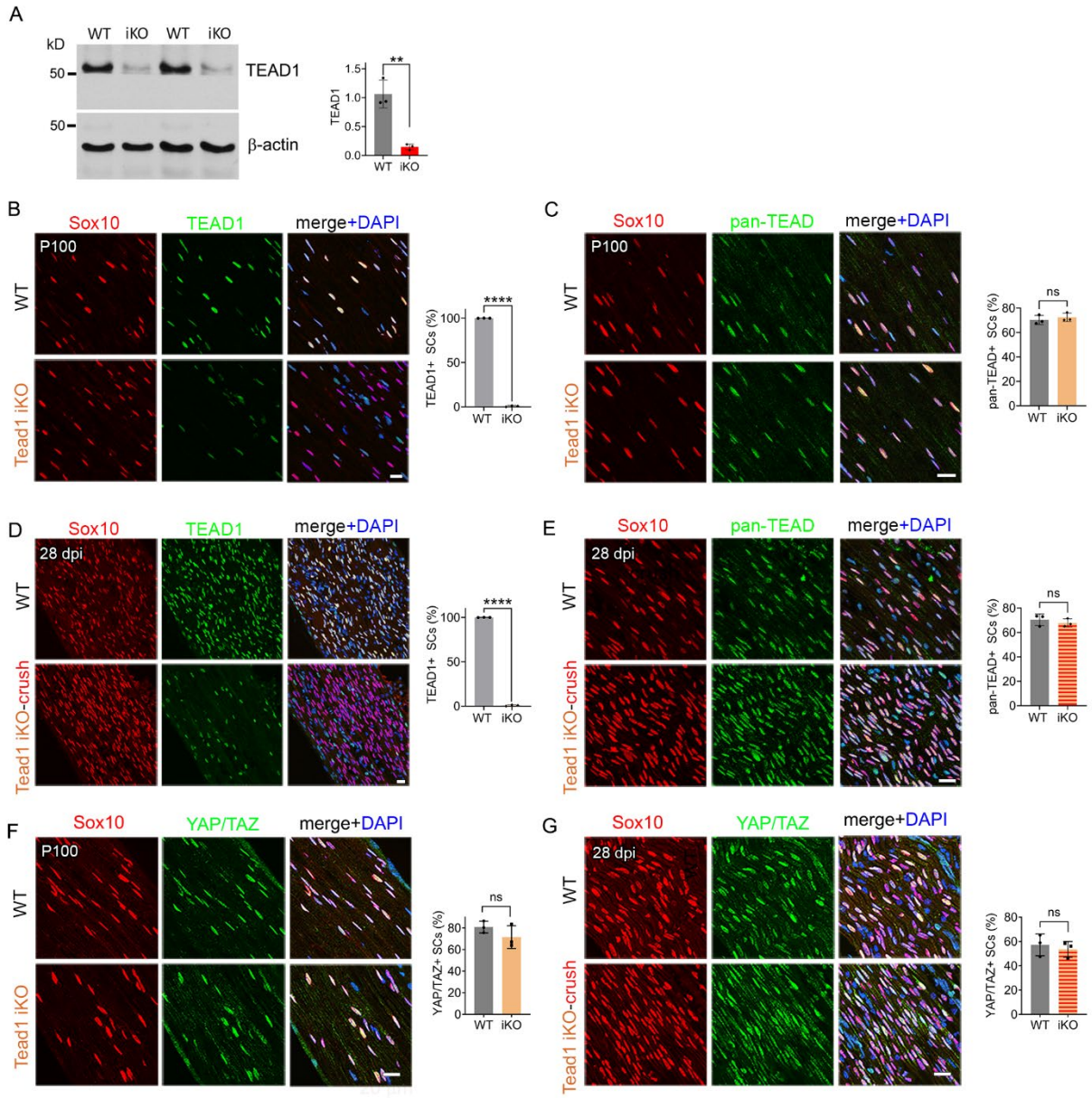

Figure 6-figure supplement 1

Expression of TEAD1, pan-TEAD and YAP/TAZ in intact and regenerating nerves of WT and *Tead1* iKO mice

(A) Western blotting of adult WT and *Tead1* iKO SN lysates with anti-TEAD1. TEAD1 expression is normalized to that of *β-actin* as an internal control, and WT expression is arbitrarily given the value 1. n = 3 mice per genotype. **$p \leq 0.01$, Student's unpaired t-test.

1088 **(B)** Immunostaining and quantification of TEAD1+ SCs on longitudinal sections of P100 WT
1089 and *Tead1* iKO SNs 3 months after tamoxifen administration. SC nuclei are identified by Sox10.
1090 All cell nuclei are marked by DAPI. n = 3 mice per genotype, ****P < 0.0001, Student's
1091 unpaired t-test. Scale bar: 20μm
1092 **(C)** Immunostaining and quantification of pan-TEAD+ SCs on longitudinal sections of P100 WT
1093 and *Tead1* iKO SNs. SC nuclei are identified by Sox10. All cell nuclei are marked by DAPI. n =
1094 3 mice per genotype. ns, p > 0.05, Student's unpaired t-test. Scale bar: 20μm
1095 **(D)** Immunostaining and quantification of TEAD1+ SCs on longitudinal sections of WT and
1096 *Tead1* iKO SNs 28 days after nerve crush. SC nuclei are identified by Sox10. All cell nuclei are
1097 marked by DAPI. n = 3 mice per genotype, ****P < 0.0001, Student's unpaired t-test. Scale bar:
1098 20μm
1099 **(E)** Immunostaining and quantification of pan-TEAD+ SCs on longitudinal sections of P100 WT
1100 and *Tead1* iKO SNs 28 days after nerve crush. SC nuclei are identified by Sox10. All cell nuclei
1101 are marked by DAPI. n = 3 mice per genotype. ns, p > 0.05, Student's unpaired t-test. Scale bar:
1102 20μm
1103 **(F)** Immunostaining of YAP/TAZ+ SCs on longitudinal sections of P100 WT and *Tead1* iKO
1104 SNs. SC nuclei are identified by Sox10. All cell nuclei are marked by DAPI. n = 3 mice per
1105 group. ns, p > 0.05, Student's unpaired t-test. Scale bar: 20μm
1106 **(G)** Immunostaining of YAP/TAZ+ SCs on longitudinal sections of WT and *Tead1* iKO SNs 28
1107 days after nerve crush. SC nuclei are identified by Sox10. All cell nuclei are marked by DAPI. n
1108 = 3 mice per group. ns, p > 0.05, Student's unpaired t-test. Scale bar: 20μm
1109
1110 **Source data 1**
1111 This zip archive contains source files for graphs in Figure 6C and 6E.
1112
1113 **Source data 2**
1114 This zip archive contains source files for graphs in Figure 6A-6G and uncropped labeled or
1115 unlabeled blots of Figure 6A.
1116
1117
1118

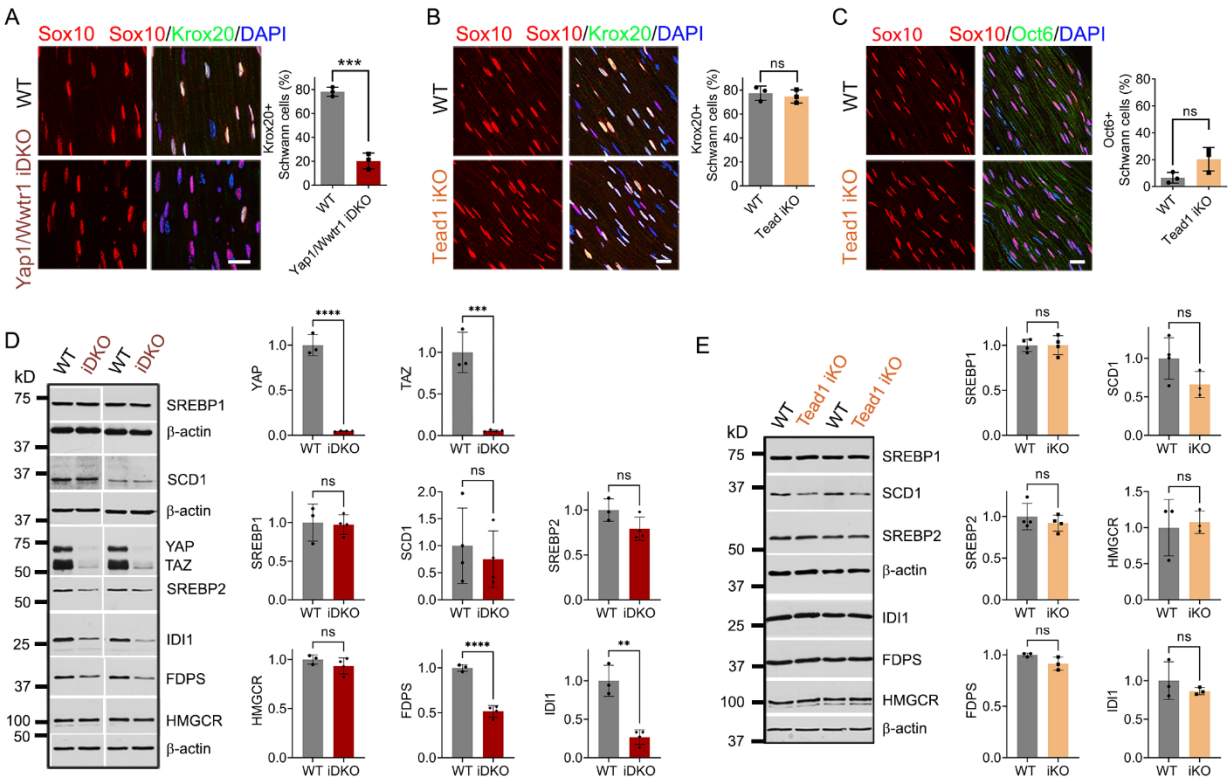

Figure 7. TEAD1 is dispensable for YAP/TAZ to maintain Krox20, FDP and IDI1 expression

(A) Immunostaining and quantification of Krox20+ SCs on longitudinal sections of WT and *Yap1/Wwtr1* iDKO SNs 2 weeks after 1st tamoxifen injection. SC nuclei are marked by Sox10. All cell nuclei are marked by DAPI. n = 3 mice per genotype, ***P < 0.001, Student's unpaired t-test. Scale bar: 20µm

(B) Immunostaining and quantification of Krox20+ SCs on longitudinal sections of WT and *Tead1* iKO SNs 6 weeks after 1st tamoxifen injection. SC nuclei are marked by Sox10. All cell nuclei are marked by DAPI. n = 3 mice per genotype, ns, p > 0.05, Student's unpaired t-test. Scale bar: 20µm

(C) Immunostaining and quantification of Oct6+ SCs on longitudinal sections of WT and *Tead1* iKO SNs 6 weeks after 1st tamoxifen injection. SC nuclei are marked by Sox10. All cell nuclei are marked by DAPI. n = 3 mice per genotype, ns, p > 0.05, Student's unpaired t-test. Scale bar: 20µm

1135 **(D)** Western blotting of WT and *Yap1/Wwtr1* iDKO SN lysates with anti-YAP, -TAZ, -SREBP1,
1136 -SCD1, -SREBP2, -HMGCR, -FDPS, and -IDI1. Protein expression is normalized to that of *β-*
1137 *actin* as an internal control, and WT expression is arbitrarily given the value 1. n = 3 or 4 mice
1138 per genotype. ns, $p > 0.05$, **$p \leq 0.01$, ***$P < 0.001$, ****$P < 0.0001$, Student's unpaired t-test.
1139 **(E)** Western blotting of WT and *Tead1* iKO SN lysates with anti-SREBP1, -SCD1, -SREBP2, -
1140 HMGCR, -FDPS, and -IDI1. Protein expression is normalized to that of *β-actin* as an internal
1141 control, and WT expression is arbitrarily given the value 1. n = 3 or 4 mice per genotype. ns, $p >$
1142 0.05, Student's unpaired t-test.
1143
1144 The following figure supplements are available for Figure 7.
1145
1146 **Source data 1**
1147 This zip archive contains source files for graphs in Figure 7A-7E and uncropped labeled or
1148 unlabeled blots of Figure 7D and 7E.
1149

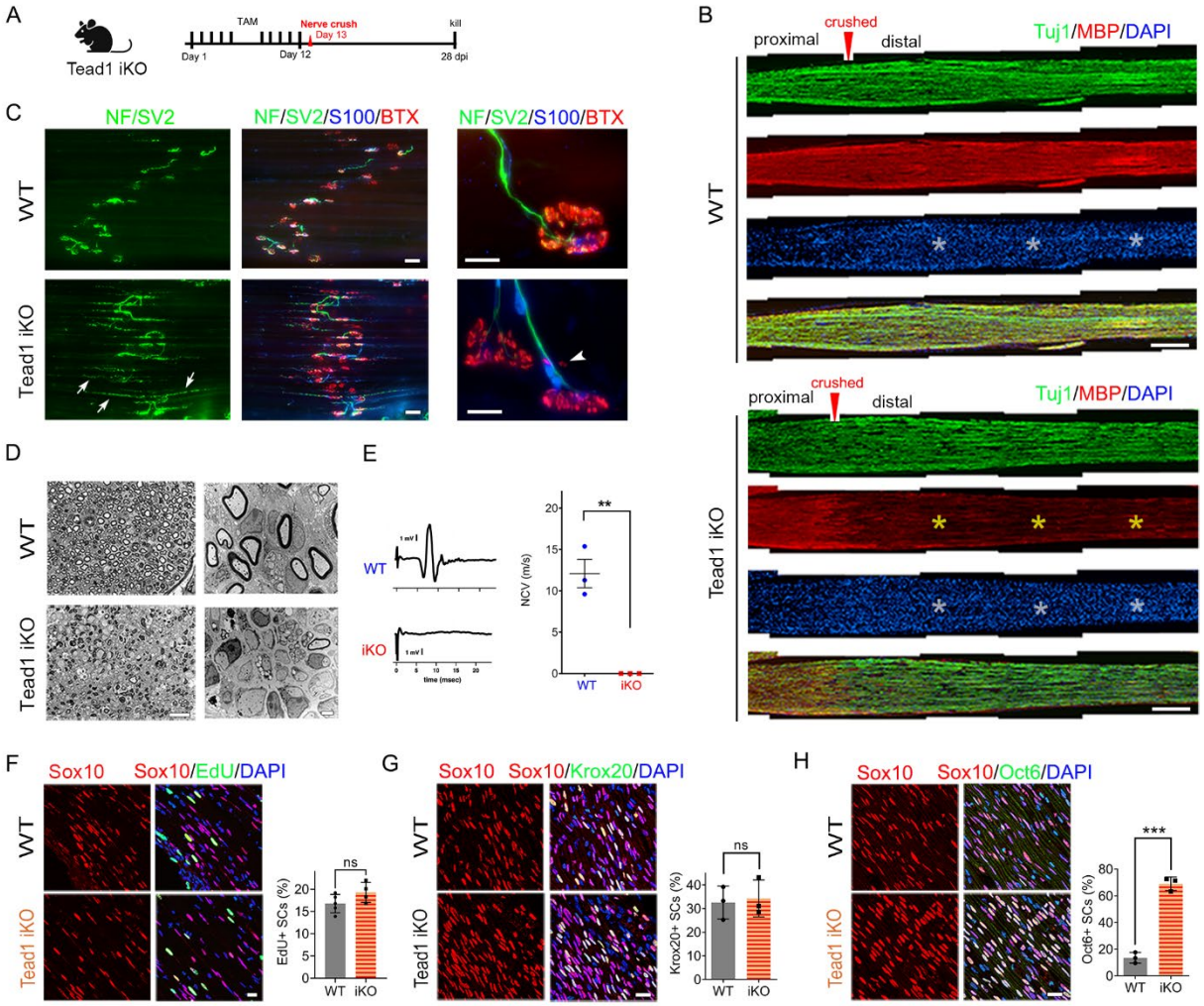

Figure 8. TEAD1 is required for functional regeneration of peripheral nerve

(A) Cartoon showing timeline of tamoxifen (TAM) injection and time of sacrifice of *Tead1* iKO mice after nerve crush.

(B) Low magnification images of longitudinal sections of ~4mm long SN segments of WT and *Tead1* iKO mice 28 days after nerve crush. Arrowheads denote crush site. Axons and myelin are marked by Tuj1 and MBP, respectively. All cell nuclei are marked by DAPI. Yellow asterisks denote the distal nerve segment of *Tead1* iKO, which almost completely lacks myelin. White asterisks denote distal segments of both WT and *Tead1* iKO, which exhibit more cells than proximal segments due to SC proliferation after injury. Scale bar: 500µm

(C) Representative low and high magnification NMJ images of WT and Tead1 iKO 28 days after nerve crush. Axon and axon terminals are marked by neurofilament (NF) and SV2 staining. SCs

1163 are marked by S100. Muscle acetylcholine receptors are marked by α-Bungarotoxin. Arrows
1164 denote examples of axon terminals that grew past NMJs in iKO. Arrowheads denote examples of
1165 extrasynaptic AChR clusters in iKO. Scale bar: 50μm (low magnification panels), 20μm (high
1166 magnification panels)
1167 **(D)** Representative semi-thin and TEM images of transverse sections of WT and *Tead1* iKO 28
1168 days after nerve crush. Scale bar: 20μm (left semi-thin panels), 2μm (right TEM panels)
1169 **(E)** Representative CMAP recordings and NCV measurements of WT and *Tead1* iKO at 28 days
1170 after nerve crush. n = 3 mice per genotype, **$p \leq 0.01$, Student's unpaired t-test.
1171 **(F)** Immunostaining and quantification of EdU+ SCs on longitudinal sections of WT and *Tead1*
1172 iKO SNs at 28 days after nerve crush. SC nuclei are marked by Sox10. All cell nuclei are marked
1173 by DAPI. n = 4-5 mice per genotype, ns, $p > 0.05$, Student's unpaired t-test. Scale bar: 20μm
1174 **(G)** Immunostaining and quantification of Krox20+ SCs on longitudinal sections of WT and
1175 *Tead1* iKO SNs at 28 days after nerve crush. SC nuclei are marked by Sox10. All cell nuclei are
1176 marked by DAPI. n = 3 mice per genotype, ns, $p > 0.05$, Student's unpaired t-test. Scale bar:
1177 20μm
1178 **(H)** Immunostaining and quantification of Oct6+ SCs on longitudinal sections of WT and *Tead1*
1179 iKO SNs at 28 days after nerve crush. SC nuclei are marked by Sox10. All cell nuclei are marked
1180 by DAPI. n = 3 mice per genotype, ns, ***$P < 0.001$, Student's unpaired t-test. Scale bar: 20μm
1181
1182 The following figure supplements are available for Figure 8.
1183
1184 **Source data 1**
1185 This zip archive contains source files for graphs in Figure 8E, 8F, 8G, 8H.
1186

1187 **Video 1. A movie showing a P55 WT and two littermates *Tead1* cKO mic**

1188